Journal of Medicinal Chemistry



Article

# 3-(-2-Carboxyethyl)indole-2-carboxylic Acid Derivatives: Structural Requirements and Properties of Potent Agonists of the Orphan G Protein–Coupled Receptor GPR17

Younis Baqi, Thanigaimalai Pillaiyar, Aliaa Abdelrahman, Olesja Kaufmann, Samer Alshaibani, Muhammad Rafehi, Saman Ghasimi, Rhalid Akkari, Kirsten Ritter, Katharina Simon, Andreas Spinrath, Evi Kostenis, Qiang Zhao, Meryem Köse, Vigneshwaran Namasivayam, and Christa E Müller

*J. Med. Chem.*, **Just Accepted Manuscript** • DOI: 10.1021/acs.jmedchem.7b01768 • Publication Date (Web): 26 Jul 2018



ACS Publications

is published by the American Chemical Society. 1155 Sixteenth Street N.W., Washington, DC 20036

*Journal of Medicinal Chemistry*

# 3-(-2-Carboxyethyl)indole-2-carboxylic Acid Derivatives: Structural Requirements and Properties of Potent Agonists of the Orphan G Protein–Coupled Receptor GPR17

Younis Baqi,[1,§] Thanigaimalai Pillaiyar,[2,§] Aliaa Abdelrahman,[2] Olesja Kaufmann,[2] Samer Alshaibani,[2] Muhammad Rafehi,[2] Saman Ghasimi,[2] Rhalid Akkari,[2] Kirsten Ritter,[2] Katharina Simon,[3] Andreas Spinrath,[3] Evi Kostenis,[3] Qiang Zhao,[4] Meryem Köse,[2] Vigneshwaran Namasivayam,[2] and Christa E. Müller[2,*]

[1]Department of Chemistry, Faculty of Science, Sultan Qaboos University, PO Box 36, Postal Code 123, Muscat, Oman.

[2]PharmaCenter Bonn, Pharmaceutical Institute, Pharmaceutical Sciences Bonn (PSB), Pharmaceutical Chemistry I, University of Bonn, An der Immenburg 4, 53121, Bonn, Germany.

[3]Institute of Pharmaceutical Biology, Section Molecular-, Cellular-, and Pharmacobiology, University of Bonn, Nußallee 6, 53115, Bonn, Germany.

[4]CAS Key Laboratory of Receptor Research, Shanghai Institute of Materia Medica, Chinese Academy of Sciences, 555 Zuchongzhi Road, Pudong, Shanghai 201203, China.

**KEYWORDS**

Agonist, Central Nervous System, GPR17, Indole, Multiple Sclerosis, Structure-Activity Relationships, Synthesis

**ABSTRACT**

The orphan receptor GPR17 may be a novel drug target for inflammatory diseases. 3-(2-Carboxyethyl)-4,6-dichloro-1*H*-indole-2-carboxylic acid (MDL29,951, **1**) was previously identified as a moderately potent GPR17 agonist. In the present study we investigated the structure-activity relationships (SARs) of **1**. Substitution of the indole 1-, 5-, or 7-position was detrimental. Only small substituents were tolerated in the 4-position while the 6-position accommodated large lipophilic residues. Among the most potent compounds were 3-(2-carboxyethyl)-1*H*-indole-2-carboxylic acid derivatives containing the following substituents: 6-phenoxy (**26**, PSB-1737, $EC_{50}$ 270 nM), 4-fluoro-6-bromo (**33**, PSB-18422, $EC_{50}$ 27.9 nM), 4-fluoro-6-iodo (**35**, PSB-18484, $EC_{50}$ 32.1 nM), and 4-chloro-6-hexyloxy (**43**, PSB-1767, $EC_{50}$ 67.0 nM). (3-(2-Carboxyethyl)-6-hexyloxy-1*H*-indole-2-carboxylic acid (**39**, PSB-17183, $EC_{50}$ 115 nM) behaved as a partial agonist. Selected potent compounds tested at human P2Y receptor subtypes showed high selectivity for GPR17. Docking into a homology model of the human GPR17 and molecular dynamic simulation studies rationalized the observed SARs.

## INTRODUCTION

G protein-coupled receptors (GPCRs) constitute one of the largest families of cell membrane receptors, which are involved in the transduction of signals from extracellular to intracellular compartments.[1] GPCRs are at present one of the most important classes of targets for marketed drugs as well as those in (pre)clinical development. It is estimated that about 30% of all approved drugs interact with GPCRs, although for only less than 10% of the known GPCRs have drugs been clinically developed so far.[2,3] Orphan GPCRs for which the physiological agonists are yet unknown or unconfirmed represent an unexploited group of potential, promising drug targets. The orphan GPCR GPR17 belongs to the δ-branch of the rhodopsin-like class A GPCR family. It is coupled to $G_q$ and $G_i$ proteins mediating intracellular calcium mobilization by phospholipase C activation and a decrease in cAMP concentrations by inhibition of adenylate cyclase. At higher agonist concentrations $G_s$ coupling can also be observed resulting in an increase in intracellular cAMP concentrations.[4] Northern blot and real time polymerase chain reaction (RT-PCR) analyses indicated a predominant expression of GPR17 in the central nervous system (CNS).[5,6] GPR17 is also expressed in organs that typically undergo ischemic damage such as heart and kidney.[7] The receptor is highly conserved in vertebrates (~ 90% identity of amino acid sequence between human and mouse or rat orthologs). GPR17 antagonists have potential for the treatment of demyelinating diseases such as multiple sclerosis based on the observation that GPR17 knockout mice showed increased myelination.[7–12] Activation of GPR17, on the other hand, might be useful for treating allergic bronchial inflammation since GPR17 knockout mice displayed an increased response to allergic stimuli.[13]

To study the (patho)physiological roles of GPR17 and to allow target validation, selective ligands, agonists and antagonists are required. Although several classes of physiological compounds have been reported to activate GPR17 including nucleotides (UDP) and nucleotide-sugars (UDP-glucose and UDP-galactose) as well as cysteinylleukotrienes (CysLTC4 and CysLTD4),[5] these data could not be confirmed by several other laboratories including ours.[4,14–17] Thus, the identity of the endogenous

ligand(s) of GPR17 still remains unresolved. Hennen et al.[4] recently reported on 3-(2-carboxy-4,6-dichloroindol-3-yl)propionic acid (MDL 29,951, **1**, Figure 1) as a synthetic agonist for GPR17, which gives a robust response and has been broadly characterized in recombinant and native cells.[4,18,19] Originally, compound **1** had been reported as an antagonist of the *N*-methyl-*D*-aspartate (NMDA) receptor interacting with the glycine binding site.[20,21] In order to obtain more potent and selective GPR17 agonists, we previously developed an improved synthesis of 4- and 6-substituted 2-carboxy-1*H*-indole-3-propionic acid derivatives employing Japp-Klingemann and Fischer indole reaction procedures starting from differently substituted aniline derivatives, and performed preliminary SAR studies.[18]

In the present study, we broadly investigated the SARs of lead structure **1** with the goal to improve its potency. Moreover, we studied the molecular interactions of this class of compounds by docking them into a homology model of GPR17 based on the X-ray structure of the related $P2Y_{12}$ receptor.

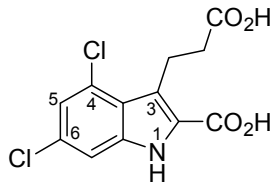


**1** (MDL 29,951)

**Figure 1.** The first reported indole derivative with GPR17-activating properties[4,18]

## RESULTS AND DISCUSSION

**Chemistry.** The desired indole derivatives were synthesized *via* Japp-Klingemann condensation followed by Fischer indole (diaza–Cope) rearrangement as depicted in Scheme 1.[4,18–21] In the first step, aniline and its derivatives (**2**) were suspended in aqueous hydrochloric acid solution (5-N) and cooled in an ice-bath with continuous stirring, followed by the dropwise addition of an aqueous sodium nitrite solution, keeping the temperature between 0–5 °C to yield the diazonium salts **3**. To

the stirred solution of **3** a previously prepared cooled solution of 2-(ethoxycarbonyl)cyclopentanone anion (**5**) was added.

**Scheme 1.** Synthesis of 3-(2-Carboxyindol-3-yl)propionic Acid Derivatives[a,b]

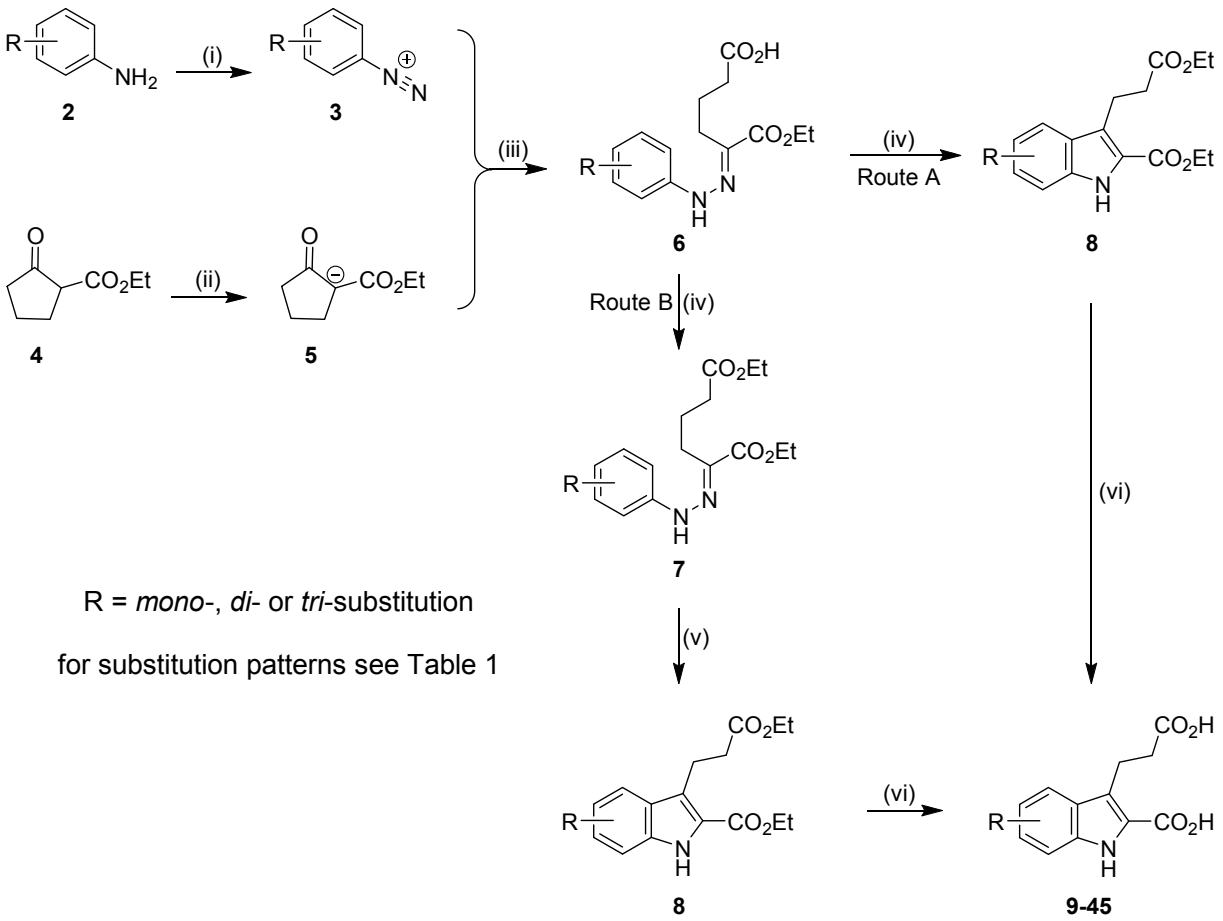


[a]Reagents and conditions: (i) HCl (5 N), $NaNO_2$ (2 equiv.), $H_2O$, 0–5 °C, 20 min; (ii) KOH (9 N) (9 equiv.), ethanol, 0–5 °C, 1h; (iii) ice, 40 °C, 1h; (iv) conc. $H_2SO_4$ (5.1 equiv.), ethanol, 100 °C, 3 h; (v); *p*-toluenesulfonic acid (*p*-TSA) ·$H_2O$ (1.5 equiv.), toluene (dry), reflux, 5 h; (vi) $LiOH·H_2O$ (3 equiv.), tetrahydrofuran (THF) : $H_2O$ (1:1 v/v), rt, 24 h, 95–100%. [b]For R see Table 1.

The resulting mixture was treated with ice and then stirred at 40 °C until the phenylhydrazine-mono-ethyl esters **6** were formed as monitored by TLC. Carboxylic acids **6** were then treated in two different ways (route A or route B, Scheme 1). In route A direct cyclization of compounds **6** producing indoles **8** was achieved by treatment with sulfuric acid in refluxing ethanol at 100 °C; however, the products were obtained in relatively low yields.[4,19–21] Subsequent saponification led to the desired indoles bearing two free carboxylic acid functions (**9–24**, Scheme 1). Following route B, compounds **6** were refluxed in ethanol in the presence of sulfuric acid to obtain the di-ethyl esters of the phenylhydrazones **7**, which were subsequently cyclized to the corresponding indole-diethyl ester derivatives **8**.[18] Finally, compounds **8** were saponified to yield the desired indoles **25–36** and **39–43** containing two carboxylic acid functions (Scheme 1, Table 1).

For unsymmetrically substituted aniline derivatives (**2**), the phenylhydrazones **7** underwent cyclization reaction furnishing two regioisomeric products (**8**). The ratio of regioisomers **8** formed was mainly dependent on the electronegativity, and on the steric hindrance of the substituents. All regioisomers bearing *di*-ester functions (compounds **8**) were separable into two regioisomeric products using silica gel column chromatography, except for one product with chlorine and bromine substitution in the 4- and 6-position, respectively (**8a**, Scheme 2). The other regioisomeric di-esters bearing fluorine and bromine, fluorine and iodine, or chlorine and alkyloxy in the 4- and 6-position, respectively, were all separable by elaborate silica gel column chromatography (for details see Supporting Information).All final product structures were confirmed by $^{1}$H- and $^{13}$C-NMR spectroscopy and high-performance liquid chromatography (HPLC) coupled to electrospray ionization mass spectrometry (ESI-MS). Purity as determined by HPLC-(UV)-ESI-MS was in all cases $\geq$ 95%.

**Table 1.** Synthesized Indole Derivatives, Analytical Data, and Potency and Efficacy to Stimulate the Human GPR17 Determined in Calcium Mobilization Assays

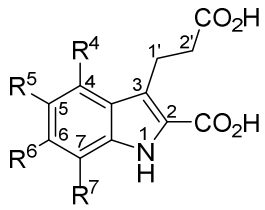

**1, 9-45, 51-60**

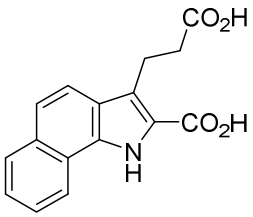

**24**

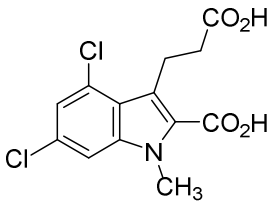

**62**

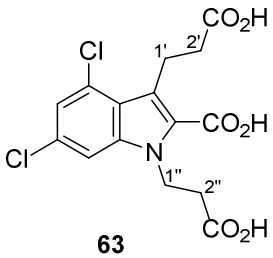

**63**

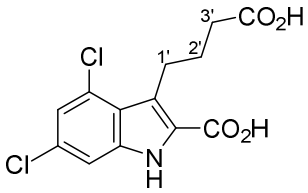

**64**

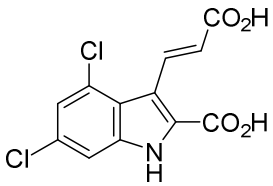

**65**

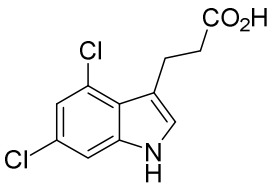

**66**

| Compd. | $R^4$ | $R^5$ | $R^6$ | $R^7$ | Yield (%)[a] | Purity (%)[b] | Human GPR17 $EC_{50}$ ± SEM (μM)[c] (% activation at indicated concentration) | Efficacy (%)[d] |
|---|---|---|---|---|---|---|---|---|
| **1**[18,20] MDL29,951 | Cl | H | Cl | H | 75 | 97.3 | **0.331** ± 0.087 | 100 |
| **9**[20] | H | H | H | H | 16 | 95.1 | **> 30** (8%) | – |
| **10**[20] | H | Cl | H | H | 25 | 95.3 | **> 30** (11%) | – |
| **11**[20] | F | H | H | H | 37 | 99.6 | **≥ 10** (44%) | – |
| **12** | H | F | H | H | 15 | 95.7 | **> 30** (9%) | – |
| **13**[20] | H | H | F | H | 45 | 99.5 | **≥ 10** (47%) | – |
| **14**[22] | H | $OCH_3$ | H | H | 17 | 95.2 | **> 30** (5%) | – |
| **15**[23] | H | isopropyl | H | H | 35 | 95.6 | **> 30** (6%) | – |
| **16**[20] | F | H | F | H | 13 | 98.9 | **7.41** ± 0.31 | 72 |

| | | | | | | | | |
|---|---|---|---|---|---|---|---|---|
| **17**[24] | $CH_3$ | H | $CH_3$ | H | 17 | 95.0 | **15.1 ±** 3.83 | 76 |
| **18**[20] | Cl | H | H | H | 30 | 98.3 | ca. **30** (52%) | – |
| **19**[20] | H | H | Cl | H | 34 | 95.3 | **3.72** ± 0.14 | 84 |
| **20**[20] | H | H | H | Cl | 35 | 100 | **> 30** (5%) | – |
| **21** | Cl | H | H | Cl | 31 | 99.7 | **> 30** (1%) | – |
| **22** | H | Cl | Cl | H | 20 | 95.5 | **> 30** (11%) | – |
| **23** | Cl | Cl | H | Cl | 15 | 95.9 | **> 30** (16%) | – |
| **24**[20] | *for structure see above* | | | | 13 | 96.1 | **> 30** (0%) | – |
| **25** | H | H | benzyl | H | 65 | 96.4 | **4.98** ± 1.09 | 80 |
| **26**[20] PSB-1837 | H | H | phenoxy | H | 41 | 99.1 | **0.270** ± 0.085 | 100 |
| **27** | $OCH_3$ | H | H | H | 94 | 100 | **> 100** (4%) | – |
| **28**[20] | H | H | $OCH_3$ | H | 99 | 100 | **> 100** (35%)[e] | – |
| **29** | H | H | Cl | Cl | 68 | 98.1 | **> 100** (5%) | – |
| **30** | H | H | Cl | F | 42 | 98.3 | **7.90** ± 1.79 | 87 |
| **31** | H | H | Br | F | 46 | 97.9 | **4.83** ± 0.49 | 98 |
| **32**[f,g] | Cl (Br) | H | Br (Cl) | H | 42 | 96.9 | **0.210** ± 0.040 | 94 |
| **33** PSB-18422 | F | H | Br | H | 13 | 98.9 | **0.0279** ± 0.0073 | 102 |
| **34** | Br | H | F | H | 11 | 98.1 | **0.624** ± 0.188 | 100 |
| **35** PSB-18484 | F | H | I | H | 17 | 99.2 | **0.0321 ± 0.0159** | 122 |
| **36** | I | H | F | H | 15 | 97.8 | **1.47 ± 0.21** | 92 |
| **37** | 4-fluorophenyl | H | Cl | H | 17 | 97.5 | **3.68** ± 0.98 | 101 |
| **38** | Cl | H | 4-fluorophenyl | H | 20 | 95.3 | **0.423** ± 0.048 | 92 |

| | | | | | | | | |
|---|---|---|---|---|---|---|---|---|
| **39**[f,h] PSB-1867 | H | H | hexyloxy | H | 47 | 97.6 | **0.115** ± 0.027 | 62 |
| **40** | pentyloxy | H | Cl | H | 27 | 97.2 | **≥ 10** | – |
| **41** | Cl | H | pentyloxy | H | 34 | 96.7 | **0.103 ± 0.039** | 98 |
| **42** | hexyloxy | H | Cl | H | 32 | 98.0 | **> 10** (40%) | – |
| **43** PSB-18183 | Cl | H | hexyloxy | H | 39 | 96.4 | **0.0670** ± 0.005 | 95 |
| **44** | octyloxy | H | Cl | H | 31 | 96.3 | > 10(25%) | – |
| **45** | Cl | H | octyloxy | H | 29 | 97.1 | **0.117 ± 0.012** | 77 |
| **51** | phenyl | H | H | H | 79 | 98.0 | **> 100** (3%) | – |
| **52** | H | H | phenyl | H | 79 | 98.1 | **0.731** ± 0.043 | 83 |
| **53** | H | H | 4-fluorophenyl | H | 49 | 99.0 | **4.02** ± 1.03 | 48 |
| **54** | H | H | 2-furanyl | H | 43 | 99.2 | **4.13** ± 1.79 | 74 |
| **55** | H | H | 2-thienyl | H | 71 | 98.1 | **9.55** ± 2.76 | 87 |
| **56** | H | H | phenyl | F | 73 | 98.3 | **3.01** ± 0.88 | 65 |
| **57** | H | H | 4-fluorophenyl | F | 74 | 98.0 | **> 100** | – |
| **58** | H | H | 2-furanyl | F | 57 | 99.2 | **14.4** ± 3.4 | 57 |
| **59** | H | H | 2-thienyl | F | 45 | 99.0 | **> 100** (21%) | – |
| **60** | phenyl | H | phenyl | H | 67 | 95.3 | **4.09** ± 2.13 | 84 |
| **62** | *for structure see above* | | | | 64 | 95.2 | **> 30** (16%) | – |
| **63** | *for structure see above* | | | | 50 | 95.0 | **5.44** ± 0.94 | – |
| **64**[25] | *for structure see above* | | | | 67 | 98.3 | **> 30** (1%) | – |
| **65**[19] | *for structure see above* | | | | 17 | 96.4 | **> 30** (22%) | – |
| **66** | *for structure see above* | | | | 25 | 96.7 | **1.68** ± 0.23 | 41 |

[a]Total isolated yield. [b]Purity of compounds was determined using high performance liquid chromatography–mass spectrometry (LC-MS) coupled to a UV detector as previously described.[26] [c]Potency to induce calcium mobilization in 1321N1 astrocytoma cells stably transfected with the

human GPR17. [d]Efficacy: the maximal effects were compared to the maximal signal induced by the lead compound **1** (at 10 μM; $EC_{50}$ 0.331). [e]Antagonistic activity was observed ($IC_{50}$ **8.40** ± 1.28 μM). [f]Obtained only as a mixture of isomers which could not be separated using normal or reversed-phase silica gel chromatography including preparative HPLC; the ratio of isomers could be determined by $^1$H-NMR spectroscopy; [g]ratio of 4-Cl,6-Br : 4-Br,6-Cl is ~ 1:1; [h]compound **39** contains 10% of the 4-hexyloxy isomer, see $^1$H NMR spectrum, Figure S1 (Supporting Information).

To introduce aromatic substituents, indole-diethyl ester derivatives bearing one or two bromo substituent(s) (**8**, **46–49**, Scheme 2)[18] were treated with different arylboronic acids under microwave-assisted Suzuki cross-coupling reaction conditions using *bis*-(triphenylphosphine)palladium(II) dichloride as a catalyst in the presence of potassium phosphate in dioxane to afford compounds **50**.

**Scheme 2.** Synthesis of Compounds **37**, **38** and **51–60** via Microwave-Assisted Suzuki Cross-Coupling Reaction of (*Di*-)Bromo-Substituted Indole Diethyl Ester Derivatives[a]

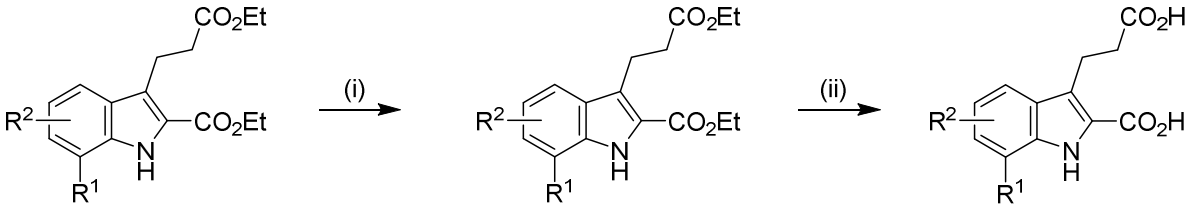


**8a,** $R^1$ = H, $R^2$ = 4,6-Cl(Br)
**46,** $R^1$ = H, $R^2$ = 4-Br
**47,** $R^1$ = H, $R^2$ = 6-Br
**48,** $R^1$ = F, $R^2$ = 6-Br
**49,** $R^1$ = H, $R^2$ = 4,6-*di*-Br

**50a,** $R^1$ = H, $R^2$ = 6-Cl,4-(4-fluorophenyl)
**50b,** $R^1$ = H, $R^2$ = 4-Cl,6-(4-fluorophenyl)
**50c,** $R^1$ = H, $R^2$ = 4-phenyl
**50d,** $R^1$ = H, $R^2$ = 6-phenyl
**50e,** $R^1$ = H, $R^2$ = 6-(4-fluorophenyl)
**50f,** $R^1$ = H, $R^2$ = 6-(2-furanyl)
**50g,** $R^1$ = H, $R^2$ = 6-(2-thienyl)
**50h,** $R^1$ = H, $R^2$ = 6-phenyl
**50i,** $R^1$ = F, $R^2$ = 6-(4-fluorophenyl)
**50j,** $R^1$ = F, $R^2$ = 6-(2-furanyl)
**50k,** $R^1$ = F, $R^2$ = 6-(2-thienyl)
**50l,** $R^1$ = F, $R^2$ = 4,6-*di*-phenyl

**37, 38, 51-60**[b]

[a]Reagents and conditions: (i) Ar–$B(OH)_2$ (1.2–2.4 equiv.), $K_3PO_4 \cdot H_2O$ (1.5–3.0 equiv.), $Pd(II)Cl_2(PPh_3)_2$ (3–6 mol%), dioxane, microwave, 150 °C, 60–90 min, 43–80%; (ii) $LiOH \cdot H_2O$ (3 equiv.), THF:$H_2O$, rt, 24 h, 95–100%. [b]For $R^1$ and $R^2$ see Table 1.

The unresolved isomeric mixture of carboxylic acid *di*-esters bearing Cl and Br atoms in the 4- and 6-position (**8a**) was treated with 4-fluorophenylboronic acid under Suzuki cross-coupling conditions (Scheme 2) to provide two separable regioisomers of the *di*-esters (**50a** and **50b**). Finally, the *di*-esters **50a–l** were saponified to yield the desired arylindoles **37**, **38**, **51–60** bearing two free carboxylic acid functions (Scheme 2, Table 1).

In order to investigate the role of the N1-H function present in the indole core we treated compound **8a** (Scheme 3), with methyl iodide or ethyl 3-iodopropanoate, respectively, in the presence of potassium carbonate in refluxing acetonitrile furnishing **61a** and **61b** in 80-85% yield. Subsequent saponification yielded **62** and **63**, the *N*-substituted derivatives of lead compound **1**, in 95-99% yield (Scheme 3, Table 1).

**Scheme 3.** Synthesis of *N*-alkylated indole derivatives **62** and **63**[a]

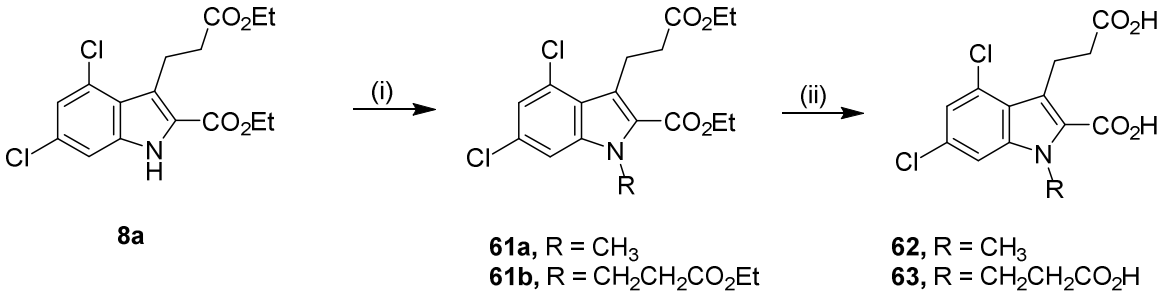


**8a**

**61a,** R = $CH_3$
**61b,** R = $CH_2CH_2CO_2Et$

**62,** R = $CH_3$
**63,** R = $CH_2CH_2CO_2H$

[a]Reagents and conditions: (i) $CH_3I$ or $BrCH_2CH_2CO_2Et$ (3 equiv.), $K_2CO_3$ (1 equiv.), $CH_3CN$, 100 °C, 18 h, 80-85%; (ii) $LiOH \cdot H_2O$ (3 equiv.), THF : $H_2O$ (1:1 v/v), rt, 24 h, 95-99%.

In a next step we wanted to probe the consequences of an increasing length, and of reduced flexibility of the alkyl side chain connected to the indole 3-position by preparing compounds **64** and **65** (Table 1).[17] Reaction of 3,5-dichloroaniline with ethyl 2-oxocyclohexanecarboxylate provided **58** in 67% yield in analogy to the synthetic route A outlined in Scheme 1 and as previously described.[20] The synthesis of **65** as a precursor of tritiated lead structure **1** has been previously described.[19]

To explore the role of the carboxylic acid function present in the 2-position of the indole moiety we regioselectively decarboxylated compound **1** at high temperature under solvent-free conditions yielding compound **66** in 25% yield (Scheme 4).

**Scheme 4.** Regioselective Decarboxylation of Lead Structure **1** to Obtain 3-(4,6-Dichloro-1*H*-indol-3-yl)propanoic acid (**66**)[a]

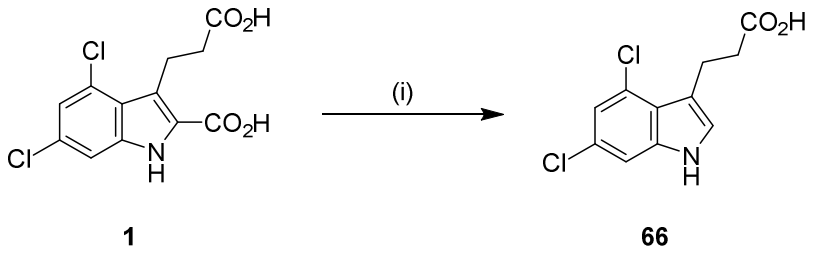


**1** **66**

[a]Reagents and conditions: (i) 275 °C, 10 min, 25%.

**Pharmacological Evaluation.** All final products were investigated for their potency to induce calcium mobilization in 1321N1 astrocytoma cells stably transfected with the human GPR17 using the calcium-chelating fluorescent dye Oregon Green® as previously described.[18] To determine compound efficacy, the maximal effects were compared to the maximal signal induced by the lead compound **1** (10 μM, $EC_{50}$ 0.331). For compounds inducing more than 50% stimulation of $Ca^{2+}$ mobilization at a test concentration of 10 μM, full concentration-response curves were determined and $EC_{50}$ values were calculated (Table 1). Compounds that did not show agonistic activity were further tested for their potency to block receptor activation by **1** (10 μM) at a high test concentration of 100 μM. Binding affinities of test compounds at GPR17 receptors were determined by

competition experiments using the GPR17 agonist radioligand [$^3$H]PSB-12150 (the $^3$H-labeled form of lead structure **1**) at membrane preparations of Chinese hamster ovary (CHO) cells stably expressing GPR17.

**Structure-activity relationships.** Previously we reported initial SARs for a small set of indole derivatives related to the lead structure **1** as agonists of GPR17.[18] Different indoles with variations in the 4- and 6-position were investigated. The indoles bearing identical substituents in both positions showed the following rank order of potency: 4,6-dibromo > 4,6-dichloro > 4,6-diiodo > 4,6-di(trifluoromethoxy) >> 4,6-dimethoxy.[18] These results indicated that the size of the substituents was important for interaction with the receptor. We had also discovered that a bulky halogen atom in the 6-position was very important for high potency, while introducing a large halogen atom in the 4-position dramatically reduced activity. In the present study 53 indole derivatives were synthesized, 35 of which are new compounds not previously described in literature. All synthesized compounds and, in addition, four commercially available indole derivatives (see Table 3) were evaluated as GPR17 receptor ligands with the goal to broadly investigate the SARs of lead structure **1** and to improve its potency on GPR17.

Steep SARs were observed. Introducing any substituent (e.g. Cl, F, OMe, or isopropyl) in the 5-position of the indole moiety abolished activity (**10**, **12**, **14**, **15**, **22**, **23**; Table 1). A fused aromatic ring, benzo[*g*]indole (**24**), connected to the 6,7-position of indole, was also not tolerated. When the chlorine atom in the 6-position of **1** was removed the potency was virtually abolished (**9**, **18**, Table 1), whereas removal of the chlorine atom in the 4-position led to an about 11-fold reduction in potency compared to **1** (**19**, $EC_{50}$ 3.72 µM, $p < 0.0001$, ****). This indicates that a substituent in the 6-position is essential, while that in the 4-position appears to be of less importance. In the 6-position a lipophilic substituent was preferred while in the 4-position a small substituent such as Cl, F or H was best. 4,6-Difluoro- and 4,6-dimethyl-substituted indoles **16** ($EC_{50}$ 7.41 µM) and **17** ($EC_{50}$ 15.1 µM) displayed low activity, again indicating that a larger lipophilic and electronegative substituent is required in the 6-position (Table 1). Any *mono*-substituted derivative in the 4- or 7-position (**11**, **20**, **27**, Table 1), or derivatives with a combination of substituents in both positions (**21**) were inactive. A

small halogen atom (fluoro) was tolerated in the 7-position while a larger one (chloro) was not.

*Mono*-substitution in the 6-position, especially with a large and lipophilic substituent, was well tolerated (**19**, $EC_{50}$ 3.72 μM; **25**, $EC_{50}$ 4.98 μM; **26**, $EC_{50}$ 0.270 μM; Table 1), while the 6-fluoro and 6-methoxy-substituted derivatives did not show activity (**13**, **28**, Table 1). Several 4,6-disubstituted indoles with different substituents were synthesized and evaluated for GPR17 activation (**32**–**38** and **40**–**45**, Table 1). The best combination was 4-fluoro-6-bromo- substitution in **33** ($EC_{50}$ 0.0279 μM) showing a 12–fold increase compared to lead structure **1** ($p$ = 0.0255, *). The 4-fluoro-6-iodo substituted derivative **35** was similarly potent ($EC_{50}$ 0.0321 μM). The corresponding regioisomers **34** and **36** were 22–fold (compare **33/34**) and 45–fold (compare **35/36**) less potent indicating again that large residues are beneficial in the 6-position but not in the 4-position of the indole core.

In the next step, even larger lipophilic substituents (benzyl, phenoxy, pentyloxy, hexyloxy, and octyloxy) were introduced into the 6-position of the indole core. We found that an ether linkage (phenoxy, **26**, $EC_{50}$ 0.270 μM) was preferable over a methylene linker (benzyl, **25**, $EC_{50}$ 4.98 μM) by >18–fold ($p$ = 0.0126, *). An aliphatic ether-linked residue (hexyloxy, **39**) was found to result in a potent compound with an $EC_{50}$ value of 0.115 μM. Next, we designed and synthesized compounds bearing a chlorine atom in the 4-position and a long aliphatic chain consisting of five, six or eight carbon atoms connected by an ether linkage to the 6-position (**41**, **43** and **45**).. Replacing the chlorine group in the 4-position by a large lipophilic group ( pentyloxy (**40**), hexyloxy (**42**), octyloxy (**44**)) was not tolerated, while replacing the chlorine atom in the 6-position by pentyloxy (41), hexyloxy (43) or octyloxy (**45**) led to an increase in potency in the following rank order (hexyloxy > pentyloxy > octyloxy), leading to one of the most potent GPR17 agonists (**43**, Table 1) with an increase in potency by ca. 5–fold compared to lead compound **1** ($EC_{50}$ 0.0670 μM, $p < 0.0001$, ***).

All of the investigated compounds that were inactive as agonists at GPR17 showed no antagonistic activity, except for compound **28** (6-OMe), which blocked GPR17 activation induced by the agonist **1** with an $IC_{50}$ value of 8.40 μM.

Finally, the aryl-substituted indole derivatives prepared by microwave-assisted Suzuki cross-

coupling reaction were evaluated and it was found that a phenyl substituent in the 6-position was preferable over a phenyl residue in the 4-position or the 4,6-*di*-phenyl-substituted derivatives (**51**, **52** and **60**, Table 1). An unsubstituted phenyl ring in the 6-position (**52**, $EC_{50}$ 0.731 μM) was slightly better than the 4-fluorophenyl (**53**, $EC_{50}$ 4.02 μM, $p = 0.0332$, *) and the thienyl (**55**, $EC_{50}$ 9.55 μM, $p = 0.0331$, *) derivative. Adding an extra fluorine atom in the 7-position of compounds **52**–**55** dramatically reduced potency (**56–59**, Table 1). Introducing a chlorine atom in the 4-position in combination with a 4-fluorophenyl residue in the 6-position was tolerated (**38**, $EC_{50}$ 0.423 μM), while switching of the two substituents (6-chloro-4-fluorophenyl, **37**) reduced potency by >8–fold ($EC_{50}$ 3.68 μM, $p = 0.0294$, *). Methylation of the indole nitrogen furnishing **62**, increasing the length of the alkyl chain on the 3-position by one methylene unit (**64**), or introducing a double bond into the side chain (**65**) all led to a significant decrease in potency compared to the lead compound **1** (Table 1). Introducing a propionic acid moiety at the indole *N*1 position (**63**) or decarboxylation (in **66**) also resulted in reduced potency compared to lead compound **1** (**63**, $EC_{50}$ 5.44 μM, $p = 0.0056$, **; **66**, $EC_{50}$ 1.68 μM, $p = 0.0054$, **).

Figure 2 summarizes the observed structure-activity relationships of the synthesized indole derivatives. A lipophilic residue in the 4- and 6-positions was found to be important for the activity, while introducing any residue in the 5- or 7-position dramatically reduced or abolished potency. We also noticed that larger lipophilic substituents are preferred in the 6-position with the following rank order of potency: hexyloxy ($EC_{50}$ 0.067 μM) ≥ phenoxy ($EC_{50}$ 0.270 μM) > I ($EC_{50}$ 0.715 μM; $p = 0.0443$, *) ≈ phenyl ($EC_{50}$ 0.731 μM) ≥ Br ($EC_{50}$ 2.24 μM) ≈ Cl ($EC_{50}$ 3.72 μM) ≈ benzyl ($EC_{50}$ 4.98 μM) >> OMe, H ($EC_{50}$ > 100 μM), while in the other positions (4, 5, or 7) (large) substituents led to a decrease or loss of potency. The *di*-ester compounds **8** showed no potency for GPR17 (data not shown) indicating the requirement of the acidic functions. The removal of the carboxylic acid group in the 2-position moderately reduced potency. The indole NH function appears to play a crucial role in GPR17 binding, it may form a hydrogen bond with the receptor protein or with a water molecule.

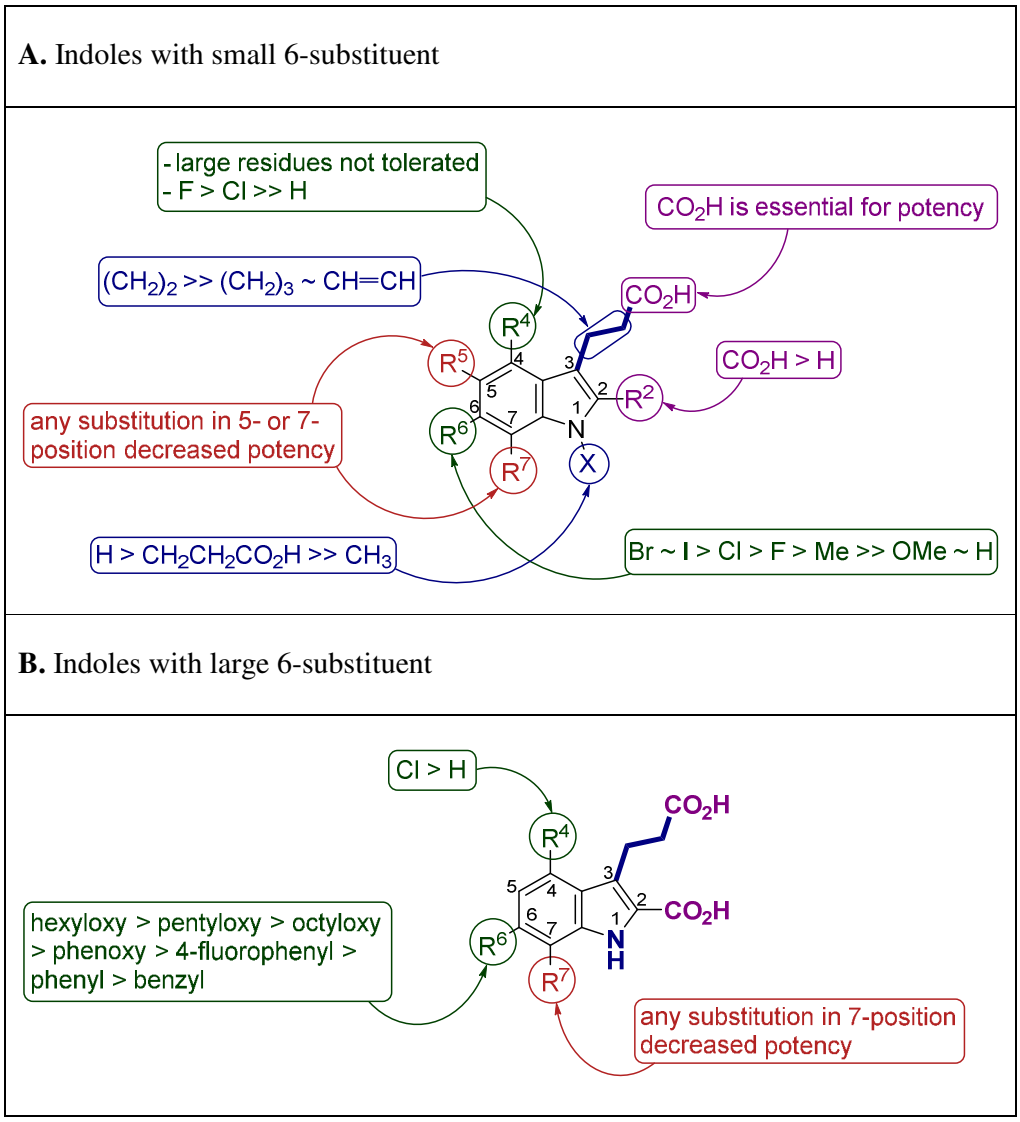


**Figure 2.** Summary of the structure-activity relationships of the synthesized indole derivatives as GPR17 agonists. **A**. Indoles with small 6-substituent. **B**. Indoles with large 6-substituent.

Small halogen atoms in the 4-position (e.g. F, Cl) in combination with larger halogen atoms (Br, I) in the 6-position increased the activity (see Figure 2A), a 6-hexyloxy chain (in **43**) was also beneficial (Figure 2B). Concentration-response curves for selected potent indole derivatives (**1**, **33**, **35**, **39**, and **43**) are provided in Figure 3.

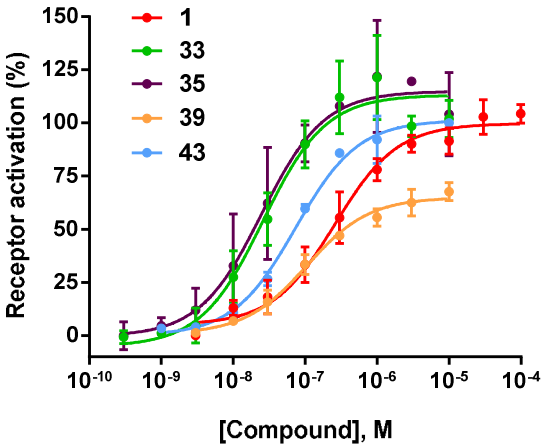


**Figure 3.** Concentration-response curves of selected indole derivatives determined in calcium mobilization assays at 1321N1 cells recombinantly expressing the human GPR17.

**Efficacy.** The maximal effect of a GPCR agonist determined in a G protein-dependent assay may be dependent on the receptor expression level or the so-called "receptor reserve".[25] In the employed 1321N1 astrocytoma cell line recombinantly expressing the human GPR17 most of the investigated indole derivatives behaved as full or nearly full agonists (70-100 % efficacy) with efficacies in the same range as lead compound **1** (set at 100 %). However, there were a few notable exceptions. The 6-methoxyindole derivative **28** appeared to display very low efficacy (35% stimulation at a high concentration of 100 µM) and actually blocked receptor activation induced by the full agonist **1** with an $IC_{50}$ value of 8.40 µM. The analog of **1** that lacked the 2-carboxylate function (**66**) also possessed low efficacy (41%). This indicates that the 2-carboxylate may be important for inducing or stabilizing the fully active conformation for G protein coupling of the receptor. Also, indoles with a large 6-substituent combined with a fluorine atom in the 7-position appeared to be less efficacious than their analogs lacking the 7-fluoro substitution (compare **56** (65% efficacy) / **52** (83%); **58** (57%) / **54** (74%)). Interestingly, this effect was not observed for the 6-Cl- and 6-Br-substituted indoles **30** (98%) and **31** (87%) bearing a 7-fluorine atom. A few indole derivatives substituted with a large, lipophilic 6-substituent but lacking a substituent in the 4-position also showed decreased efficacy, e.g. the 6-hexyloxy derivative **39** (62%) and the *p*-fluorophenyl derivative **53** (48%). It appears that the introduction of a chlorine atom in the 4-position canrestore the efficacy (see 4-chloro-6-

pentyloxyindole derivative **41**, 98%, 4-chloro-6-hexyloxyindole derivative **43**, 95%, 4-chloro-6-octyloxyindole derivative **45**, 77%). These results show the interdependence of effects on different substitution patterns possibly indicating different binding modes.

**Selectivity.** In Table 2 GPR17 agonistic activities of selected compounds are compared with their NMDA antagonistic activities previously published by Salituro and coworkers.[20,21] The SARs show that small halogen atoms, e.g., Cl, in the 6-position of the indole ring enhanced binding affinity and selectivity towards the glycine binding site over the glutamate binding site of the NMDA receptor. Especially lead compound **1** of the present study was potent and selective for the glycine binding site. Compound **1** showed similar potency in activating GPR17 as in blocking the NMDA receptor. However a bulkier group in the 6-position (e.g. phenoxy, **26**) abolished interaction with the NMDA receptors and led to selectivity for GPR17 ($EC_{50}$ 0.270 μM; NMDA receptor, $IC_{50}$ >100 μM, Table 2). These results had in fact encouraged us to design indole derivatives as GPR17 agonists focusing on bulkier substituents in the 6-position, in order to develop potent and selective GPR17 agonists.

**Table 2.** Comparison of potencies of selected indole derivatives at GPR17 and the NMDA antagonistic activities[20]

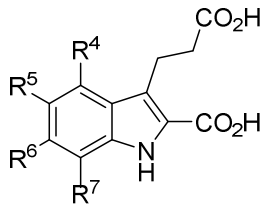


| Compd | $R^4$ | $R^5$ | $R^6$ | $R^7$ | GPR17 $Ca^{2+}$ mobilization $EC_{50}$ (μM)[a] (or % activation at indicated concentration | NMDA receptor $IC_{50}$ (μM) | |
|---|---|---|---|---|---|---|---|
| | | | | | | [$^3$H]Gly[b] | [$^3$H]CPP[c] |
| **1** | Cl | H | Cl | H | **0.331**[18] | **0.17** | **358** |
| **9** | H | H | H | H | > 30 (8) | **27** | **34** |
| **10** | H | Cl | H | H | > 30 (11) | **25** | **35** |
| **16** | F | H | F | H | **7.41** | **4** | n.a. |
| **19** | H | H | Cl | H | **3.72** | **2** | **283** |
| **20** | H | H | H | Cl | > 30 (5) | > 100 | > 1000 |
| **26** | H | H | phenoxy | H | **0.270** | > 1000 | n.a.[d] |

[a]Human receptor, for details see Table 1. [b]Competition assay vs [$^3$H]glycine at rat cortical and hippocampal membrane binding sites.[18] [c]Competition assay against [$^3$H]CCP ((3-(2-carboxypiperazin-4-y1)propyl-l-phosphonic acid) at rat cortical and hippocampal membrane glutamate binding sites.[20] [d]n.a., not available.[20]

In addition, we investigated the most potent GPR17 agonists (**1**, **33**, **35**, **39** and **43**) as potential agonists of P2Y receptor subtypes ($P2Y_1$, $P2Y_2$, $P2Y_4$, $P2Y_6$, $P2Y_{12}$, $P2Y_{14}$). The compounds were found to be inactive or only very weakly active as agonists. The highest potency was observed for **43** at the $P2Y_2$ receptor ($EC_{50} \geq 50$ μM, > 700-fold selectivity for GPR17) (see Table S1, Supporting Information). The compounds also were inactive of only weakly active in inhibiting selected P2Y

receptor subtypes ($P2Y_1$, $P2Y_2$, $P2Y_4$, $P2Y_6$).

Next we evaluated the known drugs indomethacin (**67**) and rizatriptan (**68**), the amino acid tryptophan (**69**) and the serotonin metabolite **70**. All of these indole derivatives were inactive as agonists at GPR17 (Table 3). However, indomethacin blocked GPR17 activation at high concentrations displaying an $IC_{50}$ value of 28.8 μM.

**Table 3.** Evaluation of Selected Established Drugs and Physiological Compounds with Indole Structure

| Compd | Name Function | Chemical Structure | Human GPR17 $EC_{50}$ ± SEM or % activation at 30 μM[a] | Human GPR17 $IC_{50}$ ± SEM or % inhibition at 30 μM[a] |
|---|---|---|---|---|
| **67** | Indomethacin<br>non-steroidal anti-inflammatory drug | 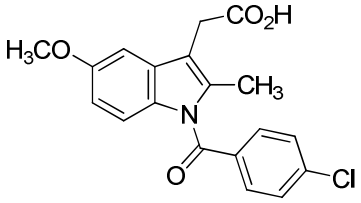 | > 30 (0%) | **28.8** ± 1.1 |
| **68** | Rizatriptan<br>5-$HT_1$ agonist | 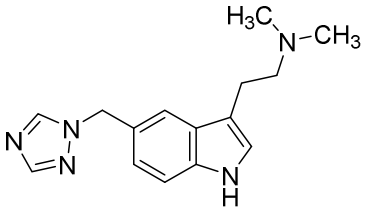 | > 30 (0%) | > 30 (27%) |
| **69** | Tryptophan<br>essential amino acid | 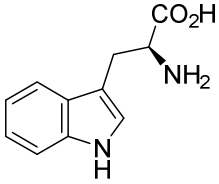 | > 30 (0%) | > 30 (1%) |
| **70** | 5-Hydroxyindole-3-acetic acid<br>main metabolite of | 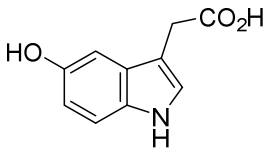 | > 30 (1%) | > 30 (7%) |

serotonin

[a]Potency to induce or inhibit calcium mobilization in 1321N1 astrocytoma cells stably transfected with the human GPR17.

A selection of the most potent indole derivatives (**1**, **33/34** (1:1 mixture), **39** and **43**) was further investigated in calcium mobilization assays at the rat and mouse GPR17 orthologues (Figure 4, Table 4). The potency of all compounds was very similar at the rat as compared to the mouse receptor. However, all four compounds were more potent at the human GPR17. The compounds (**1**, **32**) bearing a small 6-substituent (a halogen atom) were only slightly (2- to 6-fold) more potent at human as compared to rodent GPR17, and the difference was not statistically significant. However the compounds bearing an alkoxy residue in position 6 (**39**, **43**) showed large differences being 34-48-fold more potent at the human as compared to rat or mouse GPR17. This indicates that the large 6-substituent is mainly responsible for the significant species differences (human versus rodent).

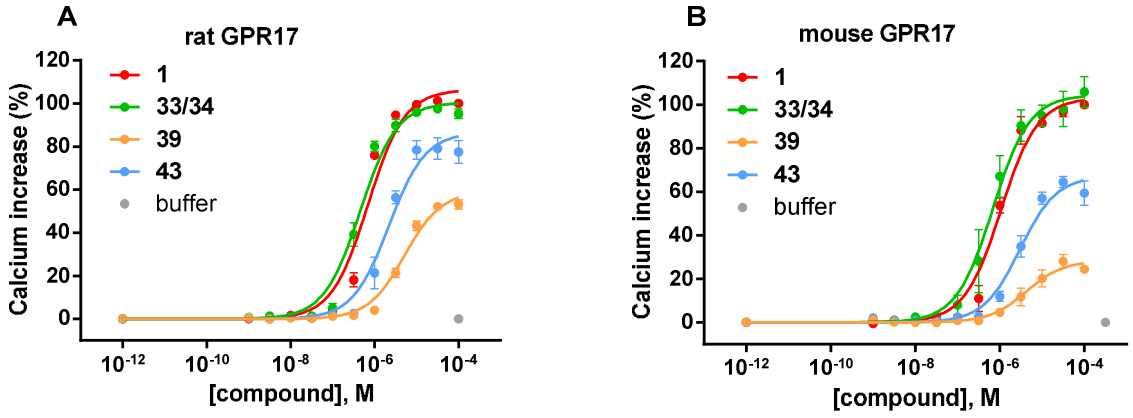


**Figure 4.** Concentration-response curves of selected indole derivatives in $Ca^{2+}$ mobilization assays performed with HEK-rat-GPR17 (**A**) and HEK-mouse-GPR17 cells (**B**). Data points represent means ± SEM from 3 independent experiments. For $EC_{50}$ values see Table 4.

**Table 4.** Comparison of GPR17 agonistic potencies of selected indole derivatives by calcium mobilization assay in different species

| Compd | Chemical Structure | Human GPR17 $EC_{50}$ ± SEM (μM)[a] (Efficacy) | Rat GPR17 $EC_{50}$ ± SEM (μM)[b] (Efficacy) | Mouse GPR17 $EC_{50}$ ± SEM (μM)[c] (Efficacy) |
|---|---|---|---|---|
| **1** | 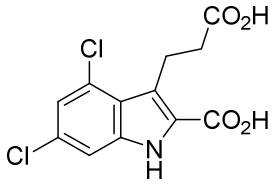 | **0.331** ± 0.087 (100 %) | **0.705** ± 0.041 (100 %) | **1.11** ± 0.18 (100 %) |
| **33/34**[d] | 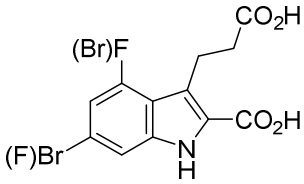 | **0.134** ± 0.023 (82 %) | **0.470** ± 0.060 (95 %) | **0.753** ± 0.194 (106 %) |
| **39**[e] | 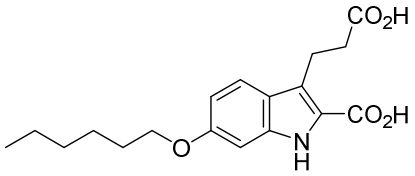 | **0.115** ± 0.027 (62 %) | **5.31** ± 0.83 (53 %) | **5.51** ± 2.19 (28 %) |
| **43** | 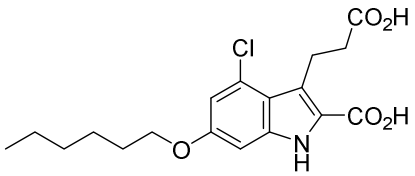 | **0.067** ± 0.005 (95 %) | **2.30** ± 0.22 (77 %) | **3.03** ± 0.17 (59 %) |

[a]Potency to induce calcium mobilization in 1321N1 astrocytoma cells stably transfected with the human GPR17. [b]Potency to induce calcium mobilization in HEK cells transfected with the rat GPR17. [c]Potency to induce calcium mobilization in HEK cells transfected with the mouse GPR17. [d]Ratio of 4-F,6-Br : 4-Br,6-F is ~ 1:1; [e]Ratio of 4-H,6-hexyloxy : 4-hexyloxy,6-H is ~ 10:1

**Homology model of the human GPR17 receptor.** As a next step, a homology model of the human GPR17 was generated based on the crystal structure of the human $P2Y_{12}$ receptor ($P2Y_{12}R$) both of which belong to the δ-family of class A GPCRs.[28] The sequence alignment between the human

GPR17 and the human $P2Y_{12}R$ is shown in Figure S18 of Supporting Information. The overall sequence identity and similarity between the human GPR17 and $P2Y_{12}$ receptor is 27.6 % and 42.9 %, respectively. The human $P2Y_{12}R$ had previously been crystallized in complex with the antagonist ethyl 6-(4-{[(benzylsulfonyl)amino]carbonyl}piperidin-1-yl)-5-cyano-2-methylnicotinate (AZD1283, PDB ID: 4NTJ) and the agonists 2-methylthio-ADP (2MeS-ADP, PDB ID: 4PXZ) and 2-methylthio-ATP (2MeS-ATP, PDB ID: 4PY0).[28,29] Meanwhile, the crystal structure of the human $P2Y_1R$ was published in complex with the antagonists 2-iodo-$N^6$-methyl-(*N*)-methanocarba-2′-deoxyadenosine-3′,5′-bisphosphate (MRS2500, PDB ID: 4XNW) and 1-(2-(2-(*tert*-butyl)phenoxy)pyridin-3-yl)-3-(4-(trifluoromethoxy)phenyl)urea (BPTU, PDB ID: 4XNV). The structures of the $P2Y_1$ receptor are both in an inactive state, and only in complex with ligands binding to two distinct, presumably allosteric binding sites. Previous attempts by Eberini *et al.* to generate a homology model for the human GPR17 had been based on the crystal structures of the human $\beta_1$-adrenergic, the human adenosine $A_{2A}$, the turkey and the human $\beta_2$-adrenergic receptors due to lacking of an X-ray structure of a closely related GPCR at that time.[30,31]

Since the $P2Y_{12}R$ belongs to the same subgroup of the δ-branch class A GPCRs as GPR17, the high resolution (2.5 Å) crystal structure of the human $P2Y_{12}$ receptor in an active state in complex with an agonist currently represents the most suitable template for generating a homology model of the human GPR17 in its active conformation. After the alignment of the human $P2Y_{12}R$ and GPR17 sequences, 500 models were generated through the homology modelling tool MODELLER.[32,33] From the 500 generated models, the presented homology model (Figure 5) was selected on the basis of the Discrete Optimized Protein Energy (DOPE) score and visual inspection. The homology model of the human GPR17 shows two disulfide bonds, the first one between Cys104 and Cys181 that is conserved among most members of the class A GPCR family and connects extracellular loop 2 (ECL2) and transmembrane 3 (TM3), and a second disulfide bridge between Cys23 and Cys269 which connects ECL3 and the *N*-terminus of GPR17.

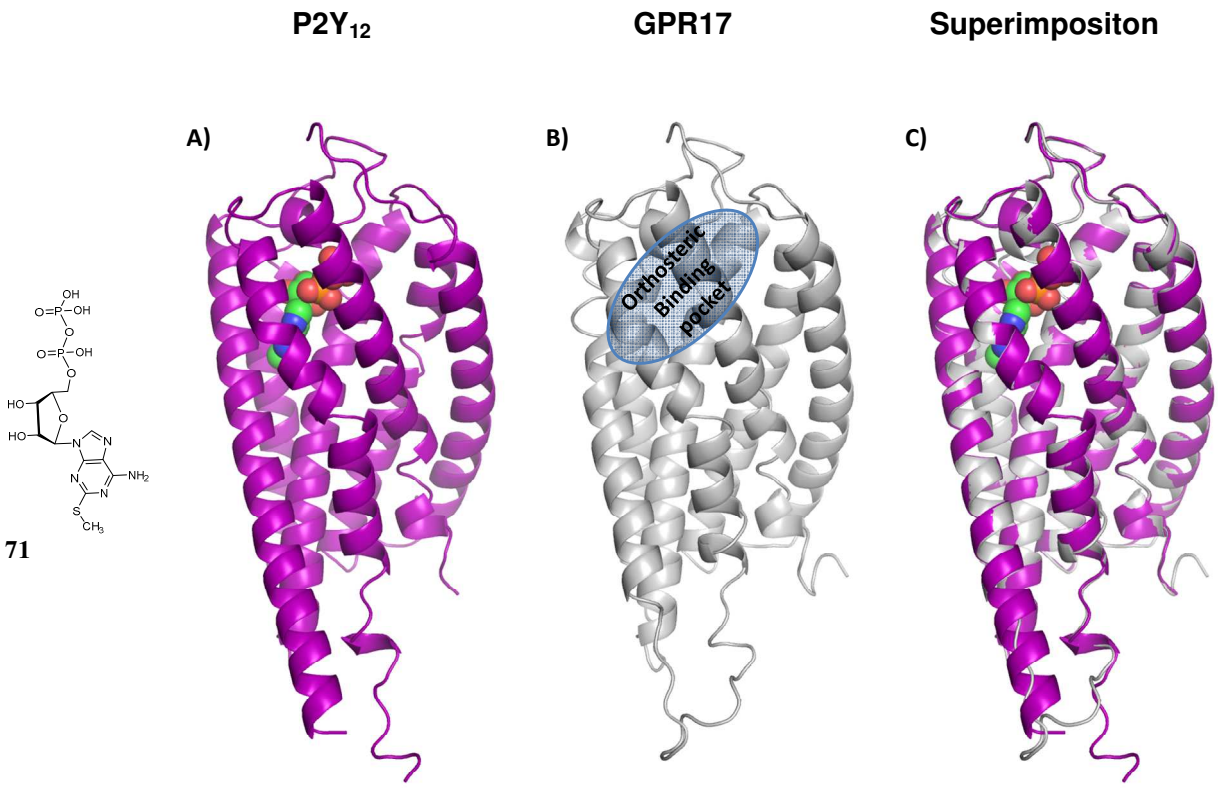


**Figure 5.** Homology model of the human GPR17 receptor. **(A)** The X-ray structure of the human $P2Y_{12}R$ (PDB ID: 4PXZ), which was used as a template for generating the homology model of the human GPR17. The $P2Y_{12}R$ agonist 2MeS-ADP (**71**) binds to the orthosteric binding site. **(B)** The homology model of the human GPR17 with a schematic representation of the putative orthosteric binding site deduced from the $P2Y_{12}R$ crystal structure. **(C)** The superimposed structures of the human $P2Y_{12}R$ and GPR17. The receptors are represented as cartoon models, the co-crystallized atoms of the ligand are depicted as spheres.

A plausible binding site with a volume of 265 $Å^3$ was identified in GPR17 using the SiteFinder module from Molecular Operating Environment (MOE 2014.09[34]). This binding site is comparable to the orthosteric binding site in the crystal structure of the human $P2Y_{12}$ receptor in complex with the agonist 2MeS-ADP (PDB ID: 4PXZ).[28] The important amino acids in the binding site of the human $P2Y_{12}R$ and the human GPR17 homology model are shown in Figure 6.

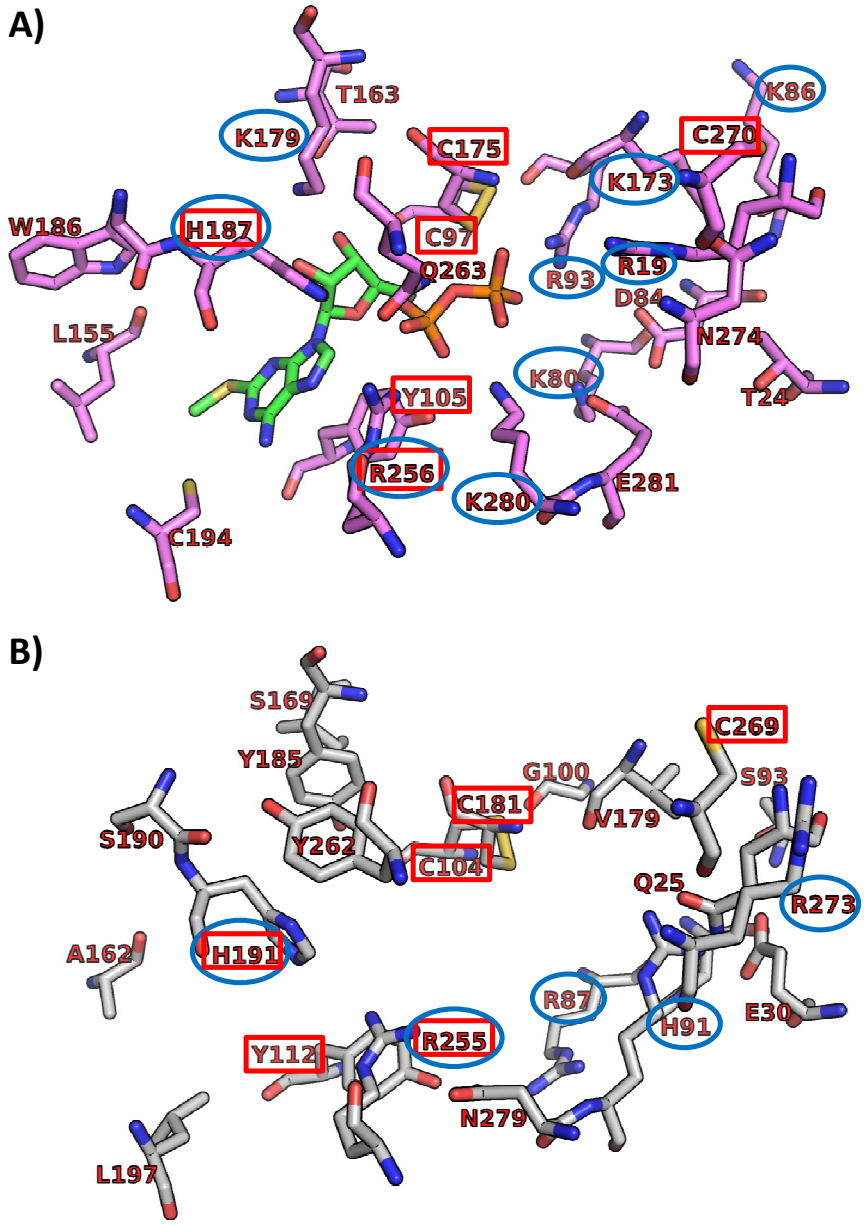


**Figure 6.** Comparison of **(A)** the orthosteric binding site of the human $P2Y_{12}R$ (PDB ID: 4PXZ), and **(B)** the putative binding site of the human GPR17. The important amino acids are shown. The conserved amino acids between the human $P2Y_{12}R$ and GPR17 are highlighted by red boxes, and the positively charged amino acids are encircled in blue. The amino acids and the cocrystallized human $P2Y_{12}$ agonist 2MeS-ADP are represented as stick models. The oxygen atoms are colored in red, nitrogen atoms in blue, sulfur atoms in yellow, chlorine in green.

A considerable similarity of the amino acids in the orthosteric binding site of the human $P2Y_{12}R$ and the proposed binding site of the human GPR17 supports the selection of the human $P2Y_{12}R$ as a template for generating a homology model of the human GPR17. However, the number of positively charged amino acid residues in the binding site of the $P2Y_{12}R$ is higher (9 residues) in comparison to the putative binding site of the human GPR17 (only 5 residues). Among the five positively charged amino acid residues in the proposed binding pocket of GPR17, one amino acid (Arg273) is exposed towards the solvent. Its lower number of positively charged amino acids may explain why nucleotides such as ADP or ATP are not binding to the human GPR17 with high affinity.[16,19]

**Molecular docking studies of the agonists.** To propose a binding mode for the new indole derivatives that were developed in the present study as agonists for the human GPR17, and to rationalize the determined SARs we selected lead compound **1** and the most potent agonist **43**. The docking and glide scores from the induced-fit molecular docking experiments, and the SARs from a previously published study[18] and from this study were taken into account.

As illustrated in Figure 7, lead compound **1** located in the putative binding site of the receptor, binds primarily through strong electrostatic and hydrogen bonding interactions. According to the putative binding pose of **1** obtained from our docking studies, the two carboxylic acid residues form strong electrostatic interactions with Arg87 and Arg255, and a hydrogen bond interaction with Asn279. Tyr112 (TM3) located below the docked pose of compound **1** likely contributes to the stabilization of the indole moiety in the putative binding pocket through aromatic π-π-interactions, and Tyr258 (TM6) positioned above agonist **1** might contribute interactions through its aromatic ring after binding of **1** inside the binding pocket. The Cl-substitution at position 4 of the indole moiety is directed towards a small hydrophobic subpocket formed by the cysteine disulfide residues Cys104-Cys181 and the residues Gly108, Phe109, Tyr112 and Leu182 in our model. The halogen atoms F, Cl or Br at position 4 of the indole agonists possibly form electrostatic interactions with the backbone of Cys104, Gly108, Phe109, Tyr112, Cys181 or Leu182.

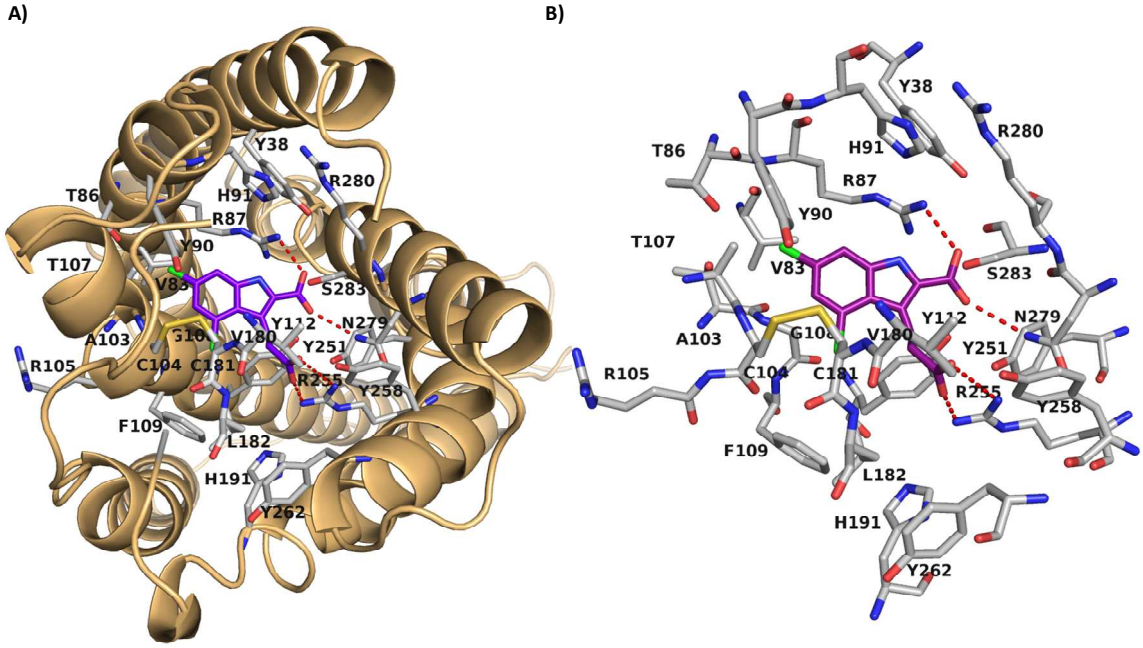


**Figure 7.** Proposed binding mode of **1** in the human GPR17 homology model (based on the human $P2Y_{12}R$ crystal structure, PDB ID: 4PXZ). **(A)** Docked pose of **1** with the important residues in the putative binding pocket of the human GPR17 receptor. **(B)** The residues important for the interaction are depicted in gray. The human GPR17 model (light brown) is displayed in cartoon representation, and the amino acid residues (gray) and compound **1** (purple) are shown as stick models. For color code see Figure 6; interactions are shown as red dotted lines.

The strong enhancement of activity by the chlorine atom in position 6 of the indole core may be explained by electrostatic interactions with Thr86 (TM2) or Thr107 (TM3) located at a distance of ~4 Å (Figure 7 A).

The putative binding pose and 2D interaction diagram of **43** are shown in Figure 8. The binding pose shows that **43** likely has a different orientation in the orthosteric binding pocket than lead compound **1**.

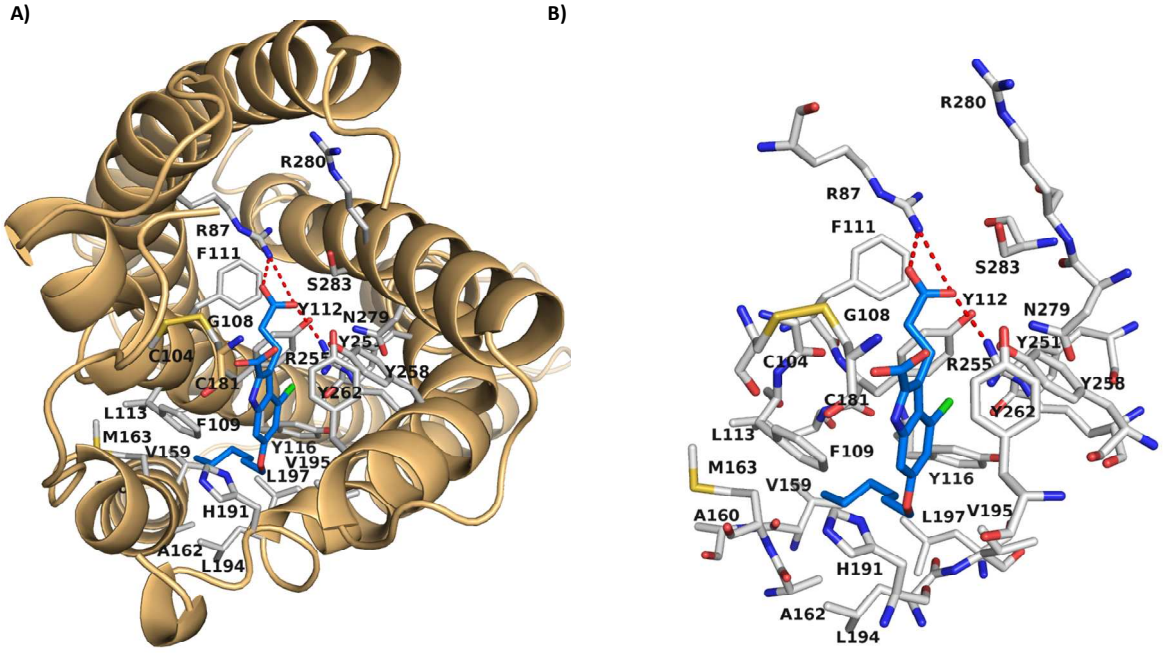


**Figure 8.** Proposed binding mode of **43** in the human GPR17 homology model (based on the human $P2Y_{12}R$ crystal structure, PDB ID: 4PXZ). (**A**) Docked pose of **43** with the important residues in the putative binding pocket of the human GPR17. (**B**) The residues important for the interaction are depicted in gray. The human GPR17 model (light brown) is displayed in cartoon representation, and the amino acid residues (gray) and compound **43** (marine blue) are shown as stick models. For color code also see Figure 6 and 7.

The summary of the SARs (see Figure 2) shows the significance of having both carboxylic acid functions and a free indole-NH group. The terminal carboxylic acid of the propanoic acid residue attached to the indole 3-position might interact with Arg87, Arg255 and Asn279 leading to electrostatic and hydrogen bond interactions. On the other hand, the carboxylic acid group in the indole 2-position probably binds below the extracellular loop 2 (ECL2), and due to the length (25 residues) and high flexibility of the ECL2 it is difficult to predict which amino acid residue of ECL2 it might bind to. The NH group of the indole moiety appears to be exposed towards the solvent and probably forms hydrogen bond interactions with water molecules. The Cl-substitution in the 4-position might form electrostatic interactions with Arg255 located at a distance of ~3.5 A, and due to the high flexibility of the arginine this interaction could easily be achieved. Tyr258 is located above the residues Arg255 and Asn279 which are likely forming important electrostatic and hydrogen bond

interactions with **43**, and Tyr258 may play an important role in maintaining the conformation of these two residues and keeping **43** in place. The hexyloxy substitution, a large lipophilic substituent at position 6, likely introduces tight hydrophobic interactions with the residues formed by Phe109, Tyr112, Leu113, Tyr116, Val159, Ala162, Met163, Leu166, Leu194, Val195 and Leu197 from TM3, TM4 and TM5. Thus, lead structure **1** and one of the most potent agonists of the present series, compound **43**, likely occupy the putative binding pocket in two different regions and orientations. Compound **1** likely binds deeper into the binding pocket, while **43** interacts with the hydrophobic residues of TM4 and TM5. A comparison of the binding pose of 2MeS-ADP in the crystal structure the human $P2Y_{12}R$ with the docked pose of **43** obtained for the human GPR17 is shown in Figure S23 (see Supporting Information). In order to verify that the agonists **1** and **43** form a stable complex with the human GPR17, molecular dynamic simulations for a time scale of 100 ns were performed. As shown in Figure S24 (see Supporting Information), for the receptor complexes the RMSD values of the $C_\alpha$ atoms rapidly reached the equilibrium phase approximately within 1.0–1.5 Å deviations from the starting structure of the complex. This suggests that the human GPR17 maintains a similar interaction profile upon binding of **1** and **43**. The trajectories from the simulations also show that the agonists **1** and **43** reside within the putative binding site throughout the simulation of 100 ns (see Supplementary Material, Video V1 and V2).

**Comparison of mouse, rat and human GPR17.** To search for a possible explanation for the observed species differences of the investigated indole derivatives (see Table 4), the amino acid sequences of the mouse, rat and human GPR17 were aligned (see Supplementary Figure S4). The human GPR17 displays high sequence identity with both the mouse and the rat GPR17 (89.7%). However, the experimental results of selected indole derivatives tested in different species (Table 4) showed that there are significant species differences for compounds **39** and **43**, which bear large lipophilic alkyl chains in position 6. Upon analyzing the sequences of rat and mouse GPR17 in comparison to the human receptor it was observed that the only variable amino acid in the identified binding site is Val195 in the human receptor, which is replaced by Ala195 in the mouse and rat GPR17 (see Supplementary Figure S5). The experimental results obtained for **39** in different species

showed that Val195 located in TM5 in the human receptor might be involved in stabilizing ligand-receptor interactions. Possibly, Val195 in the human GPR17 plays an important role in providing a strongly hydrophobic environment and orienting Arg265 to form interactions with the propionic acid group attached to the indole 3-position (**43**, $EC_{50}$ 0.0670 µM, Table 4). Its replacement by Ala195 in rat and mouse GPR17 led to a significant drop in the potency for **43** with $EC_{50}$ values of 2.21 µM (*P* = 0.0096, **) and 3.03 µM (*P* = 0.0033, **), respectively. The docked pose of **43** in the rat GPR17 model (see Figure S25, Supporting Information) showed that there is no large difference in comparison to the putative binding pose obtained for **43** in the human GPR17 model. This shows that **43** could bind to the rat GPR17 similarly as to the human GPR17 without any destabilization in the binding pocket, but the difference in potency values obtained for **43** as compared to the less hydrophobic **1** may be due to Ala195. The replacement of Ala195 in the rat and mouse GPR17 for Val in the human GPR17 does not appear to alter the interaction of **1** with the receptor, and the determined potencies are not significantly altered (see Figure 9A and Table 4). This indicates that Val195, located in TM5 of the human GPR17, is probably involved in hydrophobic interactions or might have an effect on the conformation of the amino acid Arg255 for interacting with agonists in the binding site, and thereby contributes to potency differences for the various indole derivatives with a hexyloxy group in the 6-position (**39**, **43**) at the human as compared to the rat and mouse GPR17 (see Figure 9B).

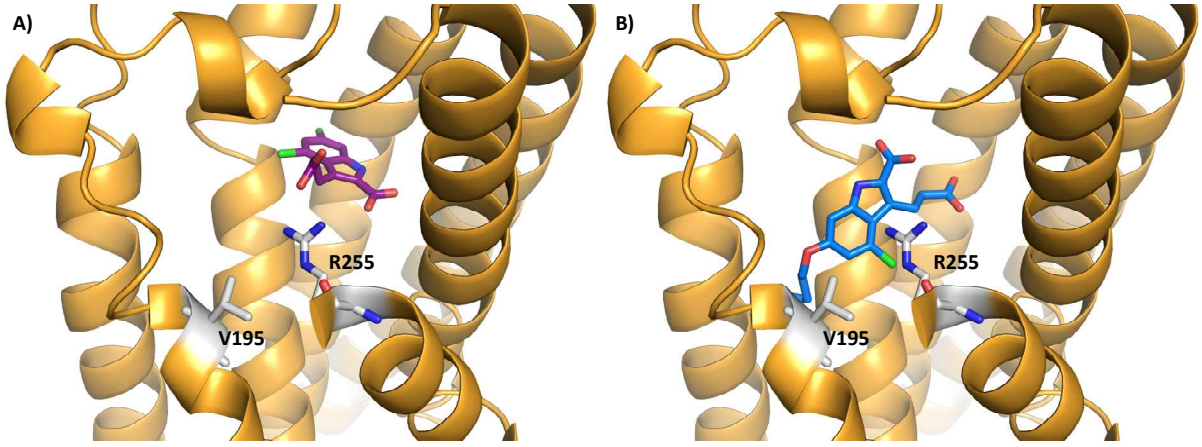

**Figure 9.** Proposed binding mode of (**A**) **1** and (**B**) **43** in the human GPR17 homology model (based on the human $P2Y_{12}R$ crystal structure, PDB ID: 4PXZ) with the amino acid residues unique in the human (Val195) as compared to the rat and mouse GPR17 and the important amino acid Arg255 interacting with the carboxylic acid group of the propionic acid residue at the indole position 3 of **1** and **43**, shown in stick representation in gray.

**Radioligand binding studies**. Finally, we performed competition binding studies using tritiated **1**, which we had previously prepared and characterized.[19] Membrane preparations obtained from recombinant CHO cells with high expression of the human GPR17 were used (see Figure 10).

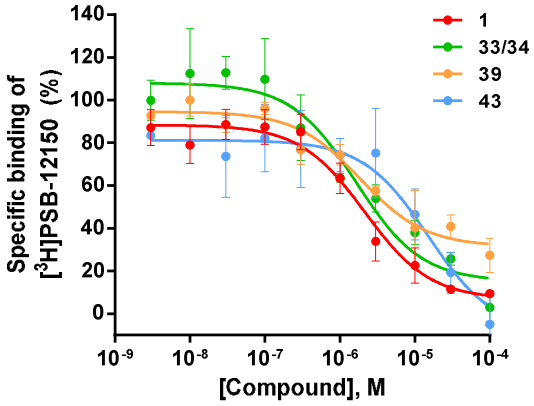


**Figure 10.** Competition experiments at membrane preparations from recombinant CHO cells expressing the human GPR17. $K_i$ values were calculated as follows: 2.45 ± 0.69 µM for compound **1**, 1.46 ± 0.28 µM for compound **33/34** (1:1), 1.50 ± 0.35 µM for compound **39**, and 13.1 ± 4.6 µM for compound **43**. Data points represent means ± SEM from 3 independent experiments, each performed in duplicates.

While compound **33/34** which is F-/Br-substituted in the 4- and 6-position of the indole core showed a similar affinity as **1**, consistent with the potencies of **1** and **33/34** in functional assays (Table 4), compounds **37** and **39**, both bearing a long hexyloxy residue in position 6, showed lower affinity towards the GPR17 conformation labeled by **1** than expected based on functional studies. This may again indicate that compounds bearing a small 6-substituent such as chlorine or bromine (**1**, **33**) bind

to a different site and stabilize a different conformation of the receptor than indoles bearing a large, lipophilic 6-substituent (**39**, **43**).

## CONCLUSIONS

In conclusion, a series of *tri*-, *tetra*- and *penta*-substituted indole derivatives (53 compounds) was synthesized and evaluated as agonists of the orphan receptor GPR17, 35 of which (**12**, **21–23**, **25**, **27**, **29–45**, **51–60**, **63** and **66**) have not been previously described in literature. In addition, four commercially available indole derivatives were investigated. 3-(2-Carboxy-indol-3-yl)propionic acid derivatives substituted in the 4- and 6-position or only the 6-position of the indole ring showed high GPR17 receptor activity. While the receptor pocket interacting with the 6-position is able to accommodate large lipophilic residues, that for the 4-position is very limited in size. Any substituent in the 5- or 7-position abolished the activity with the exception of 7-fluoro which was tolerated. An unsubstituted *N*-atom of the indole ring and an ethyl linkage between the indole 3-position and the carboxylic acid function were found to be essential for high potency.

The most potent compounds of the investigated indole derivatives exhibited $EC_{50}$ values of 27.9 nM (6-bromo-3-(2-carboxyethyl)-4-fluoro-1*H*-indol-2-carboxylic acid, **33**), 32.1 nM (3-(2-carboxyethyl)--4-fluoro-6-iodo-1*H*-indol-2-carboxylic acid, **35**), 67.0 nM (3-(2-carboxyethyl)-4-chloro-6-hexyloxy-1*H*-indole-2-carboxylic acid, **43**), and 115 nM (3-(2-carboxyethyl)-6-hexyloxy-1*H*-indole-2-carboxylic acid, **39**, partial agonist). The findings were rationalized by docking studies of **1** and **43** into a homology model of the human GPR17 based on the X-ray structure of the related ADP-activated $P2Y_{12}$ receptor in complex with agonists. The $P2Y_{12}$ receptor is the closest currently available template for generating a homology model of the human GPR17. Selected potent indole derivatives (**1**, **33/34**, **39** and **43**) were further investigated as agonists of other GPR17 orthologues (rat and mouse). While the indoles bearing a small halogen atom in position 6 were found to be similarly active in all three species, compounds with a large lipophilic residue in position 6 were much more potent at human as compared to rodent GPR17. This is probably due to the difference in a single amino acid residue in the putative orthosteric binding pocket, namely Val195 in the human,

and Ala195 in the mouse and rat GPR17. The anti-inflammatory drug indomethacin, an indole derivative, was found to block GPR17 with micromolar potency ($IC_{50}$ 28.8 μM). Some of the new compounds including **26**, **33**, **35**, **39** and **43** are useful pharmacological tools and represent new lead structures for further optimization.

## EXPERIMENTAL SECTION

### 1. Chemistry

**1.1. Material and Methods.** All commercially available chemicals were used as purchased without prior purification. Thin-layer chromatography was performed using TLC aluminum sheets silica gel 60 $F_{254}$. Synthesized compounds were visualized under UV light (254 nm). $^{1}$H- and $^{13}$C-NMR data were collected on Bruker Avance 500 MHz ($^{1}$H) or 126 MHz ($^{13}$C), respectively. $CD_3OD$ or DMSO-*d*6 was used as solvent. Chemical shifts are reported in parts per million (ppm) relative to the deuterated solvents (DMSO-*d*6), δ $^{1}$H: 2.49 ppm, $^{13}$C: 39.7 ppm, $CD_3OD$, δ $^{1}$H: 3.31, 4.78 ppm, $^{13}$C: 49.2 ppm, coupling constants *J* are given in Hertz and spin multiplicities are given as s (singlet), d (doublet), t (triplet), q (quartet), m (multiplet), br (broad). The purities of isolated products were determined by HPLC-(UV)-ESI-MS using the same procedure as previously described.[24] The purity of the compounds was determined at 254 nm and was in all cases ≥ 95%. For further proof of purity of the final compounds $^{1}$H-NMR was determined. Melting points were measured on a melting point apparatus and are uncorrected. For microwave reactions a CEM Focused Microwave Synthesizer type Discovery apparatus was used. Known compounds (**1**, **9–11**, **13**–**20**, **24**, **26**, **28, 64** and **65**) were synthesized in analogy method to the previously published procedures.[18,20]

**1.2. General Procedures for the Preparation of the Products 12, 21–23, 25, 27 and 29–45: General procedure A. (I) Preparation of Benzenediazonium Salt Solutions (Mixture I):** To a well stirred suspension of aniline derivatives (10 mmol) in 16.6 ml hydrochloric acid [5 M] at 0–5 °C was dropwise added a solution of sodium nitrite (1.38 g, 20 mmol, 2 equiv.) in 8 ml water, previously cooled to 0–5 °C in an ice bath. The addition of sodium nitrite solution was slow, in order

to keep the temperature of the mixture below 8 °C. The resulting orange-red mixture was stirred at 0–5 °C for additional 20 min in an ice bath.

**1.3. Preparation of 2-(Ethoxycarbonyl)cyclopentanone Anion Solution (Mixture II):** 2-(Ethoxycarbonyl)cyclopentanone (2.512 ml, 1.344 g, 15 mmol) was dissolved in ethanol (4.2 ml) and cooled to 0–5 °C. Then, a potassium hydroxide solution (5.040 g, 90 mmol, 6 equiv.) in water (5 ml) previously cooled to 0–5 °C was added dropwise within ca. 30 min in order to keep the temperature below 8 °C. The mixture turned to a white-milky appearance, and the final mixture was stirred at 0–5 °C for further 30 min.

**1.4. Preparation of Compounds 6:** Ice (50 g) was added to mixture II with stirring at 0–5 °C in an ice bath, followed by the addition of mixture I, and stirring continued for 1 h at 40 °C. The combined mixtures were then let to cool to rt and the pH was subsequently adjusted to 4–5 by adding hydrochloric acid (1M). The desired product was extracted with diethyl ether (3 × 50 ml). The combined organic layers were collected, dried over magnesium sulfate, filtered, and the filtrate was evaporated to dryness yielding gummy material (95–100%). This material was used without further purification for the next step.

**1.5. General procedure B. Preparation of Compounds 7:** Compound **6** (10 mmol), obtained from general procedure A, was dissolved in absolute ethanol (100 ml) followed by the addition of concentrated sulfuric acid (2.7 ml, 50.5 mmol, 5.1 equiv.). The mixture was then allowed to reflux for 1 h at 100 °C. Then the ethanol was evaporated and the residue was treated with 100 ml of ice-water. The aqueous solution was extracted with dichloromethane (3 × 50 ml); the organic layer was dried over magnesium sulfate, filtered and concentrated. The residue was purified by silica gel column chromatography using 20% of ethyl acetate in cyclohexane yielding a white solid in 85–100% yield.

**1.6. General procedure C. Indole Cyclization Reactions: Preparation of Indole *di*–Ethyl Esters (8):** A mixture of *p*-toluenesulfonic acid (2.954 g, 15 mmol, 1.5 equiv.) and 100 ml of dry toluene was refluxed for 1 h at 140 °C; water was continuously removed by means of a Dean-Stark

trap. Subsequently, 10 mmol of the starting material **7** dissolved in a minimum amount of dry toluene (ca. 15 ml) was added and the mixture was refluxed for 5 h. Then it was allowed to cool down to rt, and toluene was removed under reduced pressure and the residue was dissolved in dichloromethane and washed with water. The organic layer was dried over magnesium sulfate, filtered, and evaporated to dryness. The residue was purified by silica gel column chromatography using 20% of ethyl acetate/cyclohexane as eluent.

**1.7. General procedure D. Microwave–Assisted Suzuki Cross–Coupling Reactions: Synthesis of Compounds 37, 38, 51–60:** Compounds **8** and **46–49** (0.5 mmol), arylboronic acids (0.6–1.2 mmol, 1.2–2.4 equiv.) and potassium phosphate trihydrate (0.75–1.5 mmol, 1.5–3.0 equiv.) were mixed together in a 10 ml microwave vial. The vial was purged with Argon and bis(triphenylphosphine)palladium(II) dichloride (0.015–0.030 mmol, 3–6 mol %) and 5 ml of dry dioxane were added to the mixture. The microwave vial was capped and irradiated at 100 watt, 150 °C, under pressure up to 10 bars. Then it was allowed to cool down to rt, and toluene was removed under reduced pressure and the residue was dissolved in dichloromethane and washed with water. The organic layer was dried over magnesium sulfate, filtered, and evaporated to dryness. The residue was purified on a silica gel column chromatography using 20% of ethyl acetate/cyclohexane as eluent to yield products **50a–l** in excellent isolated yield.

**1.8. General procedure E. Indole Alkylation Reactions: Preparation of Indole *N*-Substituted di-ethyl Esters (61a and 61b).** A mixture of ethyl 4,6-dichloro-3-(3-ethoxy-3-oxopropyl)-1*H*-indole-2-carboxylate **8** (0.358 g, 1 mmol), potassium carbonate (0.138 g, 1 equiv.) and alkyl iodide (3 equiv.) in acetonitrile (10 mL) was refluxed for 18 h. The solvent was evaporated under reduced pressure and the residue was taken by ethyl acetate and washed with saturated $NaHCO_3$ solution. The organic layer was dried over sodium sulphate, filtered and concentrated under vacuum. The resulting crude sample was purified by column chromatography using 20% ethylacetate/cyclohexane as eluent to offer compounds **61a** and **61b** in 80–85% yield (Scheme 3).

**1.9. General procedure F. Saponification of Indole Diethyl Esters 8, 50 and 61a,b Yielding the Final Products 27–39**, **51–60 and 63–65:** Compound **8**, **50**, or **61a,b** (10 mmol) was dissolved

in 25 ml tetrahydrofurane (THF) with stirring at rt. Then a solution of 1.26 g of lithium hydroxide trihydrate (3 equiv.) in 25 ml water was added and the resulting mixture was left to stir at rt for 24 h. After completion of the reaction THF was removed under reduced pressure, the pH was adjusted to 4–5, and the product was extracted with diethyl ether (3 × 30 ml). The collected organic layers were dried over magnesium sulfate, filtered, and evaporated to dryness to yield the final products (**27–39**, **51–60** and **63–64**) as solids in excellent isolated yield (95–100%). The spectral data of the newly synthesized indole derivatives (**9–15**, **17**, **26**, **62**, and **64**) are provided in the supporting information.

**1.10. Synthesis of 3-(4,6-Dichloro-1*H*-indol-3-yl)propanoic acid 60.** Compound 1 (151 mg, 0.5 mmol) was melted at 275 °C for 10 min. The reaction mixture was then treated with dichloromethane and purified by column chromatography using silica gel and ethylacetate/cyclohexane as eluent to produce compound **66** in 25% yield (Table 1, Scheme 4).

**2. Spectral Data of the Novel Indole Derivatives (25**, **31**–**39**, **41**, **43**, **45**, **51**, **53**, **54**, **56**, **60**, **63**, **66**.

**6-Benzyl-3-(2-carboxyethyl)-1*H*-indole-2-carboxylic acid (25).** M.p. 252-254 °C. $^{1}$H-NMR (DMSO-$d_6$) δ 2.28 (t, $^{3}J$ = 8.4 Hz, 2H, H-1′), 3.24 (t, $^{3}J$ = 8.4 Hz, 2H, H-2′), 4.37 (s, 2H, $CH_2$), 6.74 (dd, $^{3}J$ = 7.1 Hz, $^{5}J$ = 0.7 Hz, 1H, H-4″), 7.07 (dd, $^{3}J$ = 8.3 Hz and $^{4}J$ = 1.3 Hz, 2H, H-2″), 7.14 (pt, $^{3}J$ = 8.3 Hz and $^{4}J$ = 1.2 Hz, 1H, H-5 and $^{3}J$ = 7.16 Hz, $^{4}J$ = 2.3 Hz, 1H, H-7), 7.24 (t, $^{3}J$ = 7.6 Hz, 2H, H-3″), 7.31 (dd, $^{3}J$ = 8.3 Hz, $^{4}J$ = 0.9 Hz, 2H, H-4), 11.64 (s, 1H, NH), 12.60 (s, 2H, $2CO_2H$). $^{13}$C-NMR (DMSO-$d_6$) δ 21.2 (C-1′), 36.2 (C-2′), 38.6 ($CH_2$), 111.3 (C-7), 121.8 (C-3), 122.1 (C-5), 124.3 (C-3a), 124.4 (C-4), 125.0 (C-2), 126.0 (C-4″), 128.4 (C-2″), 128.5 (C-3″), 134.1 (C-7a), 137.0 (C-6), 141.1 (C-1″), 163.2 (2′-$CO_2H$), 173.9 (2-$CO_2H$). LC-MS (*m*/*z*): 341.34 $[M+NH_4^+]^+$, 324.31 $[M+H]^+$, 322.21 $[M-H]^-$. Purity (LC-MS): 96.4 %.

**6-Bromo-3-(2-carboxyethyl)-7-fluoro-1*H*-indole-2-carboxylic acid (31).** M.p. 253-255 °C. $^{1}$H-NMR (DMSO-$d_6$) δ 2.49 (m, 2H, H-1′), 3.24 (t, $^{3}J$ = 8.1 Hz, 2H, H-2′), 7.22 (dd, $^{3}J$ = 8.6 Hz and $^{4}J_{HF}$ = 5.9 Hz, 1H, H-5), 7.47 (d, $^{3}J$ = 8.7 Hz, 1H, H-4), 12.12 (s, 1H, NH), 12.63 (br, 2H, $2CO_2H$). $^{13}$C-NMR (DMSO-$d_6$) δ 20.0 (C-1′), 35.0 (C-2′), 102.1 (d, $^{2}J_{CF}$ = 16.5 Hz, C-6), 117.9 (d, $^{3}J_{CF}$ = 3.8 Hz, C-5), 122.4 (C-3), 123.1 (C-4), 124.8 (d, $^{2}J_{CF}$ = 13.9 Hz, C-7a), 126.5 (C-2), 130.4 (d, $^{3}J_{CF}$ = 5.4 Hz,

C-3a), 145.9 (d, $^{1}J_{CF}$ = 246.3 Hz, C-7), 162.7 (2′-$CO_2H$), 173.9 (2-$CO_2H$). LC-MS (*m/z*): 347.31 $[M+NH_4^+]^+$, 330.34 $[M+H]^+$, 330.24 $[M-H]^-$. Purity (LC-MS): 97.9 %.

**6(4)-Bromo-3-(2-carboxyethyl)-4(6)-chloro-1*H*-indole-2-carboxylic acid (32).** M.p. 270-272 °C. $^1$H-NMR (DMSO-$d_6$) δ 2.46 (t, $^{3}J$ = 7.1 Hz, 4H, H-1′), 3.50 (t, $^{3}J$ = 7.1 Hz, 4H, H-2′), 7.24, 7.31, 7.43, 7.53 (each d, $^{4}J$ = 1.6 Hz, 4H, H-5 and H-7), 11.95 (s, 2H, 2NH), 12.69 (br, 4H, 4$CO_2H$). $^{13}$C-NMR (DMSO-$d_6$) δ 20.0, 20.2 (2C, C-1'), 36.3 (2C, C-2'), 111.8, 114.4 (2C, C-7), 115.2, 116.4 (C-4 or C-6), 121.0, 121.4 (2C, C-3), 122.5, 123.4 (2C, C-2), 123.0, 123.9 (2C, C-5), 126.5, 126.8 (C-4 or C-6), 127.5 128.9 (2C, C-3a), 137.3, 137.9 (2C, C-7a), 162.7 (2C, 2′-$CO_2H$), 173.6 (2C, 2-$CO_2H$). LC-MS (*m/z*): 365.08 $[M+NH_4^+]^+$, 348.18 $[M+H]^+$, 346.26 $[M-H]^-$. Purity (LC-MS): 96.9%.

**6-Bromo-3-(2-carboxyethyl)-4-fluoro-1H-indole-2-carboxylic acid (33)** M.p. 248-250 °C. $^1$H NMR (600 MHz, DMSO-$d_6$) δ 2.47 (d, *J* = 8.0 Hz, 2H, H-1′), 3.32 (s, 2H, H-2′), 7.03 (d, *J* = 10.4 Hz, 1H, H-7), 7.38 (s, 1H, 5-H), 11.89 (s, 1H, 1-NH), 12.73 (br, 2H, 2COOH). $^{13}$C-NMR (DMSO-$d_6$) *δ* 20.9 (C-1′), 35.5 (C-2′), 108.2 (C-5), 111.7 (C-7), 116.2 (C-6), 119.6 (C-3a), 125.4 (C-3), 138.6 (C-2), 156.2 (C-7), 157.8 (4-C), 162.6 (2′-$CO_2H$), 173.7 (2-$CO_2H$). LC-MS (*m/z*): 331 $[M+H]^+$. Purity (LC-MS): 98.9%.

**4-Bromo-3-(2-carboxyethyl)-6-fluoro-1H-indole-2-carboxylic acid (34).** M.p. 236-238 °C. $^1$H NMR (600 MHz, DMSO-$d_6$) δ 2.50 (s, 2H, H-1′), 3.67 (m, 2H, H-2′), 7.16 (dd, *J* = 9.2, 2.3 Hz, 1H, H-5), 7.24 (dd, *J* = 9.2, 2.3 Hz, 1H, H-7), 11.67 (s, 1H, 1-NH). 11.90 (s, 2H, 2COOH). $^{13}$C-NMR (DMSO-$d_6$) *δ* 19.7 (C-1′), 36.2 (C-1′), 97.7 (C-7), 113.6 (C-5), 114.9 (C-3a), 121.5 (C-3), 126.5 (C-7a), 136.9 (C-2), 158.5 (4-C), 160.4 (6-C), 162.6 (2′-$CO_2H$), 173.6 (2-$CO_2H$). LC-MS (*m/z*): 331 $[M+H]^+$. Purity (LC-MS): 98.1%.

**3-(2-Carboxyethyl)-4-fluoro-6-iodo-1H-indole-2-carboxylic acid (35).** M.p. 230-232 °C. $^1$H NMR (600 MHz, DMSO-$d_6$) δ 2.48 (m, 2H, H-1′), 3.32 (m, 2H, H-2′), 7.12 (d, *J* = 10.4 Hz, 1H, H-5), 7.57 (s, 1H, H-7), 11.96 (s, 1H,1-NH), 12.66 (s, 2H, 2COOH). $^{13}$C-NMR (DMSO-$d_6$) δ 21.0 (C-1′), 35.6 (C-2′), 87.6 (C-7), 113.1 (C-5), 119.6 (C-3), 125.1 (C-3a), 139.4 (C-7a), 156.1 (C-6), 157.8 (C-2), 160.4 (4-C), 162.7 (2′-$CO_2H$), 173.7 (2-$CO_2H$). LC-MS (m/z): 378 $[M+H]^+$. Purity (LC-MS): 99.2%.

**3-(2-Carboxyethyl)-6-fluoro-4-iodo-1H-indole-2-carboxylic acid (36)** M.p. 237-239 °C $^{1}$H NMR (600 MHz, DMSO-$d_6$) δ 2.47 (d, $J$ = 6.2 Hz, 2H, H-1′), 3.66 (m, 2H, H-2′), 7.17 (dd, $J$ = 9.2, 2.3 Hz, 1H, H-7), 7.47 (dd, $J$ = 9.0, 2.3 Hz, 1H, H-5), 11.81 (s, 1H, NH), 12.94 (s, 2H, 2COOH). $^{13}$C-NMR (DMSO-$d_6$) δ 18.9 (C-1′), 36.4 (C-2′), 86.7 (C-4), 98.1 (C-7), 120.3 (C-5), 123.9 (C-3a), 126.6 (C-7a), 136.3 (C-2), 160.3 (C-6), 162.7 (2′-$CO_2$H), 173.6 (2-$CO_2$H). LC-MS (m/z): 378 $[M+H]^+$. Purity (LC-MS): 97.8%.

**3-(2-Carboxyethyl)-6-chloro-4-(4-fluorophenyl)-1*H*-indole-2-carboxylic acid (37).** M.p. 246-248 °C. $^{1}$H-NMR (DMSO-$d_6$) δ 2.30 (m, 2H, H-1′), 2.93 (m, 2H, H-2′), 6.82 (d, $J$ = 2.0 Hz, 1H, H-5), 7.23 (t, $J$ = 8.7 Hz, 2H, H-3″ and H-5″), 7.48 (m, 3H, H-2″, H-4″ and H-7), 11.80 (s, 1H, NH), 12.45 (br, 2H, 2$CO_2$H). $^{13}$C-NMR (DMSO-$d_6$) δ 19.4 (C-1′), 34.7 (C-2′), 111.2 (C-7), 115.0 (C-3″ and C-5″), 121.5 (C-3), 123.2 (C-5), 125.9 (C-7, C-2), 128.4 (C-4), 130.8 (C-3a), 135.8 (C-2″ and C-6″), 136.9 (C-1″), 137.3 (C-7a), 161.1 (C-4″), 162.9 (2′-$CO_2$H), 173.3 (2-$CO_2$H). LC-MS (*m/z*): 362 $[M+1]^+$. Purity (LC-MS): 97.5%.

**3-(2-Carboxyethyl)-4-chloro-6-(4-fluorophenyl)-1*H*-indole-2-carboxylic acid (38**). M.p. 266-268 °C. $^{1}$H-NMR (DMSO-$d_6$) δ 2.52 (d, $J$ = 3.3 Hz, 2H, H-1′), 3.73 – 3.25 (m, 2H, H-2′), 7.29 (t, $J$ = 8.6 Hz, 2H, H-3″ and H-5″), 7.35 (d, $J$ = 1.5 Hz, 1H, H-5), 7.54 (d, $J$ = 1.5 Hz, 1H, H-7), 7.69 (dd, $J$ = 8.5, 5.3 Hz, 2H, H-2″ and H-4″), 11.92 (s, 1H, NH), 12.52 (br, 2H, 2$CO_2$H). $^{13}$C-NMR (DMSO-$d_6$) δ 20.3 (C-1′), 36.3 (C-2′), 109.5 (C-7), 115.9 (C-3″ and C-5″), 119.9 (C-3), 120.8 (C-5), 122.51 (C-7) 126.2 (C-2), 129.0 (C-4), 136.1 (C-3a), 136.5 (C-2″ and C-6″), 138.0 (C-7a), 161.2 (C-4″), 162.8 (2′-$CO_2$H), 173.8 (2-$CO_2$H). LC-MS (*m/z*): 362 $[M+1]^+$. Purity (LC-MS): 95.3%.

**3-(2-Carboxyethyl)-6-(hexyloxy)-1*H*-indole-2-carboxylic acid (39).** M.p. 175-176 °C. $^{1}$H-NMR (DMSO-$d_6$): δ 0.89 (m, 3H, H-6″), 1.31 (m, 4H, H-4″, H-5″), 1.42 (m, 2H, H-3″), 1.70 (m, 2H, H-2″), 2.47 (m, 1H, H-1′), 3.20 (m, 2H, H-2′), 3.94 (t, $J$ = 6.5 Hz, 2H, H-1″), 6.68 (dd, $J$ = 8.8 and 2.3 Hz, 1H, H-5), 6.80 (d, $J$ = 2.2 Hz, 1H, H-7), 7.51 (d, $J$ = 8.8 Hz, 1H, H-4), 11.16 (s, 1H, NH), 12.33 (br, 2H, 2$CO_2$H). $^{13}$C-NMR (DMSO-$d_6$) δ 14.0 (C-6″), 20.11 (C-1′), 22.14 (C-5″), 25.3 (C-4″), 28.8 (C-3″), 31.1 (C-2″), 35.2 (C-2′), 67.7 (C-1″), 94.7 (C-3), 111.3 (C-2), 120.0–123.7 (4C, C-7, C-4, C-

5, C-3a), 137.21 (C-6), 157.46 (C-7a), 163.16 (2′-$CO_2H$), 174.09 (2-$CO_2H$). LC-MS (*m/z*): $[M+H]^+$ 334.07. Purity (LC-MS): 97.6%.

**3-(2-Carboxyethyl)-4-chloro-6-(pentyloxy)-1H-indole-2-carboxylic acid (41).** M.p. 227-229 °C. $^1$H NMR (600 MHz, DMSO-$d_6$) δ 0.89 (t, *J* = 7.1 Hz, 3H, H-5″), 1.60 (m, 4H, H-4″ and H-3″), 1.90 (m, 2H, H-2″), 2.50 (m, 2H, H-1′), 3.62 (m, 2H, H-2′), 3.95 (t, *J* = 6.5 Hz, 2H, H-1″), 6.73 (d, *J* = 2.1 Hz, 1H, H-5), 6.79 (d, *J* = 2.1 Hz, 1H, H-7), 11.54 (s, 1H, 1-NH), 12.51 (s, 2H, 2COOH). $^{13}$C-NMR (DMSO-$d_6$) *δ* 14.0 (C-5″). 20.3 (C-4″), 22.0 (C-3″), 27.8 (C-2″), 28.4 (C-1′), 36.3 (C-2′), 68.1 (C-1″), 94.4 (C-3), 112.1 (C-5), 117.9 (C-4), 121.3 (C-7), 124.3 (C-3a), 126.8 (C-5), 138.3 (C-7a), 156.9 (C-6), 162.9 (2′-$CO_2H$), 173.80 (2-$CO_2H$). LC-MS (*m/z*): 354 $[M+H]^+$. Purity (LC-MS): 96.7%.

**3-(2-Carboxyethyl)-4-chloro-6-hexyloxy-1*H*-indole-2-carboxylic acid (43).** M.p. 205-207 °C. $^1$H-NMR (DMSO-$d_6$) δ 0.85 (m, 3H, H-6″), 1.25 (m, 4H, H-4″, H-5″), 1.43 (m, 2H, H-3″), 1.71 (m, 2H, H-2″), 2.41 (m, 2H, H-1′), 3.46 (m, 2H, H-2′), 3.95 (t, *J* = 6.5 Hz, 2H, H-1″), 6.73 (d, *J* = 2.1 Hz, 1H, H-5), 6.79 (d, *J* = 2.1 Hz, 1H, H-7), 11.54 (s, 1H, NH), 12.51 (br, 2H, 2$CO_2H$). $^{13}$C-NMR (DMSO-$d_6$) δ 14.0 (C-6″), 20.3 (C-1′), 22.1 (C-5″), 25.2 (C-4″), 28.6 (C-3″), 31.1 (C-2″), 36.27 (C-2′), 68.1 (C-1″), 94.3 (C-3), 112.0 (C-2), 117.9 (C-7), 121.3 (C-6), 124.3 (C-5), 126.8 (C-3a), 138.3 (C-4), 156.9 (C-7a), 162.8 (2′-$CO_2H$), 173.7 (2-$CO_2H$). LC-MS (*m/z*): 368 $[M+H]^+$, 350 $[M-NH_4^+]^-$. Purity (LC-MS): 96.4%.

**3-(2-Carboxyethyl)-4-chloro-6-(octyloxy)-1H-indole-2-carboxylic acid (45).** M.p. 229-231 °C. $^1$H NMR (600 MHz, DMSO-$d_6$) δ 0.99 (m, 4H, H-8″ and H-7″), 1.50 (m, 8H, H-6″, H-5″, H-3″ and H-3″), 1.88 (m, 2H, H-2″), 2.48 (m, 2H, H-2′), 3.57 (m, 2H, H-1′), 3.95 (t, *J* = 6.5 Hz, 2H, H-1″), 6.73 (d, *J* = 2.1 Hz, 1H, H-5), 6.80 (d, *J* = 2.1 Hz, 1H, H-7), 11.51 (s, 1H, 1-NH), 12.52 (s, 2H, 2COOH). $^{13}$C-NMR (DMSO-$d_6$) *δ* 14.0 (C-8″), 20.3 (C-7″), 22.2 (C-6″), 25.6 (C-5″), 28.7 (C-4″), 28.7 (C-3″), 28.8 (C-2″), 31.3 (C-1′), 36.3 (C-2′), 68.1 (C-1″), 94.4 (C-7), 112.0 (C-2), 117.9 (C-5), 121.1 (C-3a), 126.7 (C-6), 126.7 (C-3), 138.3 (C-7a), 156.8 (C-6), 163.0 (2′-$CO_2H$), 173.8 (2-$CO_2H$). LC-MS (*m/z*): 396 $[M+H]^+$. Purity (LC-MS): 97.1%.**3-(2-Carboxyethyl)-6-phenyl-1*H*-indole-2-carboxylic acid (52).** M.p. 238-239 °C. $^1$H-NMR (DMSO-$d_6$) δ 2.54 (m, 2H, H-2′), 3.28 (m, 2H, H-1′), 7.35 (m,

2H, 4-H, 5-H), 7.46 (m, 2H, H-2″, H-6″), 7.60 (m, 1H, 4″-H), 7.63 (m, 2H, 3″-H, 5″-H), 7.75 (m, 1H, 7-H), 11.55 (s, 1 H, NH), 12.50 (br, 2H, $2CO_2H$). $^{13}$C-NMR (DMSO-$d_6$) δ 20.1 (C-2′), 35.3 (C-1′), 110.2 (C-7), 119.2 (C-5), 121.1 (C-4), 121.4 (C-3), 124.8 (C-3a), 126.6 (C-2), 127.0 (C-3″, C-5″), 127.2 (C-4″), 129.1 (C-3″, C-6″), 136.8 (C-7a), 137.2 (C-6), 141.3 (C-1″), 163.1 (2′-$CO_2H$), 174.1 (2-$CO_2H$). LC-MS (*m/z*): 310 $[M+H]^+$, 308 $[M-H]^-$. Purity (LC-MS): 98.1 %.

**3-(2-Carboxyethyl)-6-(4-fluorophenyl)-1*H*-indole-2-carboxylic acid (53).** M.p. 250-252 °C. $^1$H-NMR (DMSO-$d_6$) δ 2.53 (t, 2H, $^3J$ = 8.0 Hz, H-1′), 3.28 (t, 2H, $^3J$ = 8.5 Hz, H-2′), 7.28 (tt, 2H, $^3J$ = 8.9 Hz and $^3J_{HF}$ = 2.2 Hz, H-2″), 7.32 (dd, 1H, $^3J$ = 8.5 Hz and $^4J$ = 1.6 Hz, H-5), 7.55 (dd, 1H, $^4J$ = 1.6 Hz and $^5J$ = 0.6 Hz, H-7), 7.67 (ddd, 2H, $^3J$ = 8.9 Hz, $^3J_{HF}$ = 5.5 Hz and $^4J$ = 2.2 Hz, H-3″), 7.74 (d, 1H, $^3J$ = 8.5 Hz, H-4), 11.51 (s, NH), 12.50 (br, 2H, $2CO_2H$). $^{13}$C-NMR (DMSO-$d_6$) δ 20.1 (C-1′), 35.3 (C-2′), 110.2 (C-7), 115.8 (d, $^2J$ = 21.3 Hz, C-3″), 119.1 (C-4), 121.1 (C-5), 121.4 (C-3), 124.9 (C-2), 126.6 (C-3a), 128.9 (d, $^3J_{CF}$ = 7.5 Hz, C-2″), 136.0 (C-7a), 136.7 (C-6), 137.8 (d, $^4J_{CF}$ = 1.3 Hz, C-1″), 161.8 (d, $^1J_{CF}$ = 242.5 Hz, C-4″), 163.2 (2′-$CO_2H$), 174.1 (2-$CO_2H$). LC-MS (*m/z*): 345.41 $[M+NH_4^+]^+$, 328.28 $[M+H]^+$, 326.11 $[M-H]^-$. Purity (LC-MS): 99.0%.

**3-(2-Carboxyethyl)-6-(furan-2-yl)-1*H*-indole-2-carboxylic acid (54).** M.p. 223-225 °C. $^1$H-NMR (DMSO-$d_6$) δ 2.52 (t, 2H, $^3J$ = 7.5 Hz, H-1′), 3.25 (t, 2H, $^3J$ = 7.5 Hz, H-2′), 6.58 (dd$^3J$ = 3.3 Hz and $^4J$ = 1.8 Hz, 2H, H-2″), 6.88 (dd, $^3J$ = 3.3 Hz and $^3J$ = 0.7 Hz, 1H, H-3″), 7.41 (dd, $^3J$ = 8.5 Hz and $^4J$ = 1.5 Hz, 1H, H-5), 7.67 (dd, $^3J$ = 1.4 Hz, $^4J$ = 0.8 Hz, 1H, H-7), 7.69 (d, $^3J$ = 8.5 Hz, 1H, H-4), 7.72 (dd, $^3J$ = 1.8 Hz and $^4J$ = 0.7 Hz, 1H, H-4″), 11.52 (s, NH), 12.49 (s, 2H, $2CO_2H$). $^{13}$C-NMR (DMSO-$d_6$) δ 20.0 (C-1′), 35.2 (C-2′), 105.4 (C-2″), 106.7 (C-3″), 112.2 (C-7), 116.3 (C-4), 121.1 (C-5), 121.7 (C-3), 125.0 (C-2), 126.6 (C-3a), 127.0 (C-7a), 136.3 (C-6), 142.7 (C-4″), 154.1 (C-1″), 163.1 (2′-$CO_2H$), 174.1 (2-$CO_2H$). LC-MS (*m/z*): 317.15 $[M+NH_4^+]^+$, 300.19 $[M+H]^+$, 298.27 $[M-H]^-$. Purity (LC-MS): 99.2%.

**3-(2-Carboxyethyl)-7-fluoro-6-phenyl-1*H*-indole-2-carboxylic acid (56).** M.p. 259-261 °C. $^1$H-NMR (DMSO-$d_6$) δ 2.54 (t, $^3J$ = 7.6 Hz, 2H, H-1′), 3.28 (t, $^3J$ = 7.3 Hz, 2H, H-2′), 7.15 (dd, $^3J$ = 8.3 Hz and $^4J_{HF}$ = 6.6 Hz, 1H, H-5), 7.38 (tt, $^3J$ = 7.4 Hz, $^4J$ = 1.3 Hz, 1H, H-4″), 7.48 (t, $^3J$ = 7.5 Hz, 2H, H-3″), 7.57 (d, $^3J$ = 8.0 Hz, 1H, H-4), 7.59 (dd, $^3J$ = 8.2 Hz, $^4J$ = 1.3 Hz, 2H, H-2″), 12.10 (s,

NH), 12.72 (br, 2H, 2$CO_2$H). $^{13}$C-NMR (DMSO-$d_6$) δ 20.1 (C-1′), 35.1 (C-2′), 116.7 (d, $^4J_{CF}$ = 2.5 Hz, C-4), 121.5 (C-5), 122.2 (C-3), 122.3 (d, $^2J_{CF}$ = 8.8 Hz, C-6), 125.2 (d, $^2J_{CF}$ = 15.0 Hz, C-7a), 125.5 (C-2), 127.6 (C-4″), 128.7 (C-3″), 129.2 (d, $^4J_{CF}$ = 2.5 Hz, C-2″), 130.1 (d, $^3J_{CF}$ = 5 Hz), 135.8 (C-1″), 146.1 (d, $^1J_{CF}$ = 247.5 Hz), 161.3 (2′-$CO_2$H), 172.3 (2-$CO_2$H). LC-MS (m/z): 345.41 $[M+NH_4^+]^+$, 328.29 $[M+H]^+$, 326.13 $[M-H]^-$. Purity (LC-MS): 98.3 %.

**3-(2-Carboxyethyl)-4,6-diphenyl-1*H*-indole-2-carboxylic acid (60).** M.p. 243-245 °C. $^1$H-NMR (DMSO-$d_6$) δ 2.07 (m, 2H, H-2′), 2.83 (m, 2H, H-1′), 7.09 (d, $^2J$ = 1.6 Hz, 1H, H-7), 7.34 (t, $^3J$ = 7.4 Hz, 1H, Phenyl ring), 7.44 (m, 7H, Phenyl ring), 7.66 (d, $^2J$ = 0.9 Hz, 2H, H-5), 7.68 (d, $J$ = 1.6 Hz, 1H, Phenyl ring), 11.72 (s, 1H, NH); 12.33 (br, 2H, 2$CO_2$H). $^{13}$C-NMR (DMSO-$d_6$) δ 20.3 (C-2′); 34.9 (C-1′), 109.5 (C-4), 120.9 (C-6), 121.7 (C-3), 123.8 (C-2), 125.5 (C-3a), 127.0 (C-2″, C-6″), 127.3 (C-4‴), 127.5 (C-4″), 128.0 (C-3‴, C-5‴), 129.0 (C-3″, C-5″), 129.1 (C-2‴, C-6‴), 135.4 (C-7a), 137.3 (C-4), 137.4 (C-6), 140.8 (C-1″), 141.0 (C-1‴), 163.1 (2′-$CO_2$H), 173.4 (2-$CO_2$H). LC-MS (*m/z*): 386 $[M-NH_4^+]^+$, 366 $[M+H]^+$, 384 $[M-H]^-$. Purity (LC-MS): 95.3 %.

**1,3-Bis-(2-carboxy-ethyl)-4,6-dichloro-1*H*-indole-2-carboxylic acid (63).** M.p. 229 °C. $^1$H-NMR (DMSO-$d_6$) δ $^1$H NMR (DMSO-$d_6$) δ 2.49 (m, 2H), 2.65 (t, $J$ = 7.25 Hz, 2H), 3.44 (t, $J$ = 8.1 Hz, 2H), 4.65 (t, $J$ = 7.25 Hz, 2H), 7.20 (d, $J$ = 1.60 Hz, 1H, H-7), 7.76 (d, $J$ = 1.55 Hz, 1H, H-5), 12.69 (br, H, 3$CO_2$H). $^{13}$C-NMR (DMSO-$d_6$) δ 20.63 (C-1'), 34.74 (C-1''), 36.31 (C-2′, C-2″), 110.47 (C-2, C-7), 121.18 (C-6, C-3), 127.19 (C-5), 128.75 (C-4), 129.03 (C-3a), 138.64 (C-7a), 162.92 (2-$CO_2$H), 172.35, 173.66 (2′-$CO_2$H, 2″-$CO_2$H). LC-MS (*m/z*): 375 $[M+H]^+$. Purity (LC-MS): 95.0 %.

**3-(4,6-Dichloro-1*H*-indol-3-yl)propanoic acid (66).** $^1$H-NMR (DMSO-$d_6$) δ 2.56 (m, 2H, H-2′), 3.12 (m, 2H, H-1′), 7.04 (d, $J$ = 1.45 Hz, 1H, H-7), 7.22 (d, $J$ = 2.45 Hz, 1H, H-2), 7.36 (d, $J$ = 1.45 Hz, 1H, H-5), 11.20 (1-NH), 12.06 (br, H, $CO_2$H). $^{13}$C-NMR (DMSO-$d_6$) δ 21.4 (C-1'), 35.6 (C-2′), 110.6 (C-2), 113.9 (C-7), 119.0 (C-6), 122.4 (C-3), 125.3 (C-5), 125.5 (C-4), 125.6 (C-3a), 137.9 (C-7a), 173.2 (2′-$CO_2$H). LC-MS (*m/z*): 258 $[M+H]^+$. Purity (LC-MS): 96.7 %.

**3. Biological assays**

### 3.1. Calcium ($Ca^{2+}$) mobilization assays.

Activation of human GPR17 was determined in 1321N1 astrocytoma cells stably transfected with the human GPR17. Measurements were performed using a Novostar® microplate reader. Calcium assays were performed according to published procedures.[35] 1321N1 human astrocytoma cells stably expressing the human GPR17 were harvested with 0.05 % trypsin / 0.02 % EDTA and rinsed with culture medium (DMEM containing 10% fetal bovine serum, 1% penicillin-streptomycin and 800 µg/ml G418). The cells were kept at 37°C with 5 % $CO_2$ for 45 min and then centrifuged at 200*g* and 4°C for 5 min. Then the cells were incubated for 1 h at 25°C in Krebs-Ringer-HEPES (KRH) buffer pH 7.4 containing 3 µM Oregon Green BAPTA-1/AM and 1 % Pluronic® F127. The cells were subsequently rinsed three times with KRH buffer, diluted and plated into 96-well plates with clear bottoms at a density of approximately 16,000 cells/well and left for 20 min. Fluorescence intensity was measured at 520 nm for 30 s with 0.4 s intervals. Buffer or test compounds were injected sequentially into separate wells using the automatic pipetting device. Compounds that were inactive as agonists were subsequently tested for antagonistic activity. The cells were preincubated with the test compound (test solutions were prepared in DMSO) at a high concentration of 100 µM (final DMSO concentration was 1%) and subsequently activated by the addition of agonist **1** (1 µM, corresponding to its $EC_{80}$ value). For potent antagonists, full concentration-inhibition curves were determined.

Intracellular calcium ($Ca^{2+}$) mobilization in rat and mouse GPR17-expressing cells was quantified with the Calcium 5 Assay Kit (Molecular Devices). Briefly, mouse GPR17- and rat GPR17-HEK293 cells, respectively, were seeded at a density of 60,000 cells per well into black poly-D-lysine-coated 96-well tissue culture plates with clear bottom. Cells were loaded with the Calcium 5 indicator dye for 40 min and according to the manufacturer's instructions the intracellular calcium mobilization was detected with the FlexStation 3 Benchtop Multimode Plate Reader.[4] Data analysis was performed using GraphPad Prism (Version 6.02). Concentration-response data were fitted by non-linear regression to estimate $EC_{50}$ values (Prism 6.02).

At least three independent experiments were performed, each in duplicates. The unpaired t-test was used for statistical comparisons (*, $p<0.05$; **, $p<0.01$; ***, $p<0.005$; ****, $p<0.001$).

**3.2. Radioligand binding assays versus [³H]PSB-12150.** Binding affinities of test compounds at the human GPR17 were determined by competition experiments using [³H]PSB-12150, a tritiated version of **1**. The precursor of the radioligand was synthesized in our laboratory, and was custom-labeled by Quotient Bioscience, U.K., to obtain [$^3$H]PSB-12150 (17 Ci/mmol). Membrane preparations and radioligand binding assays were performed as previously described.[19] In brief, the reaction mixture containing 10 mM $MgCl_2$, 25 nM [³H]PSB-12150, membranes of CHO cells stably expressing the human GPR17 (CHO-FTIR-hGPR17), and increasing concentrations of test compound was incubated for 60 min at 25 °C. After separation of membrane-bound radioligand from free radioligand by rapid filtration through GF/B glass fiber filters (Whatman, Dassel, Germany), the radioactivity was measured using liquid scintillation counting (Tri-Carb® 2810 TR, PerkinElmer, Inc., USA). Nonspecific binding was determined in the presence of 100 μM of unlabeled PSB-12150. Data were analyzed using Graph Pad Prism Version 6.0 (San Diego, CA, USA). $K_i$ values were calculated using the Cheng-Prusoff equation and a $K_D$ value of 1190 nM. Three independent experiments, each in duplicate were performed.

**3.3. Calcium ($Ca^{2+}$) mobilization assays at P2Y receptors.** The potency of the compounds was determined by assessing their ability to induce calcium mobilization in 1321N1 astrocytoma cells stably transfected with the human $P2Y_1$, $P2Y_2$, $P2Y_4$, or $P2Y_6$ receptor using a Flexstation III (Molecular Devices GmbH, Biberach an der Riss, Germany) microplate reader. The procedure has been described before.[36]

**3.4. β-Arrestin translocation assays at P2Y receptors.** Selectivity assessments of test compounds at the $P2Y_{12}$ and $P2Y_{14}$ receptors were done using β-arrestin translocation assays with CHO cells stably transfected with the respective human P2YR subtypes, as described before.[37]

**4. Three-dimensional structural modeling of human and rat GPR17 receptors.** A homology model of the human GPR17 was created based on the X-ray structure of the human $P2Y_{12}$R. The

crystal structure of the human $P2Y_{12}R$ complex with the agonist 2MeS-ADP (PDB ID: 4PXZ) was downloaded from Research Collaboratory for Structural Bioinformatics (RCSB) Protein Data Bank (PDB) (http://www.rcsb.org/).[38] The amino acid sequences of human and rat GPR17 with the accession number Q13304-2 and Q09QM4, respectively, were retrieved from UniProt sequence database (http://www.uniprot.org/).[39] The sequence alignment between the template and the target sequence was performed using Clustal Omega.[40] The alignment was visually interpreted and manually fixed to further improve the alignment. The resulting alignment was used as input for generating homology models of human and rat GPR17 using MODELLER 9.12.[33,34] From the 500 generated models, the presented homology models were selected on the basis of the Discrete Optimized Protein Energy (DOPE) score included in MODELLER. Ramachandran Plot and PROSA II profile analysis confirmed the overall structural quality and sequence−structure compatibility of the selected homology models of human and rat GPR17 (Supplementary Information Figure S2, S3).[41–43]

**5. Docking studies.** The generated homology model of the human GPR17 was used for the docking procedure using Induced Fit Docking (IFD) and Glide as implemented in Schrödinger release 2017.[43–45] During the docking simulations, the receptor and the ligands were fully flexible. The possible binding site was identified using the SiteFinder module from Molecular Operating Environment (MOE 2014.09).[34] Prior to docking, the homology models of human and rat GPR17 was prepared using the Protein Preparation Wizard module at pH 7.4 and with forcefield Optimized Potentials for Liquid Simulations Version 3 (OPLS3) implemented in Schrödinger 2017.[44–46] In the first step of flexible docking, module IFD, Glide ligand docking of the selected molecules was performed by removing the side chains of the amino acids in the selected binding pocket. In the second step of docking, the Prime was applied to refine the nearby residues and optimize the side chains. In the final step of the docking simulation, the ligand was redocked into all induced fit protein structures that were within 30 kcal/mol of the lowest energy structure by using the Glide XP scoring function. A grid center with the cubic grid side length of 10 Å was specified on the basis of the transformed position of the agonist 2MeS-ADP from the human $P2Y_{12}R$. Thus, in the docking

simulation, we limited the possible docking area and therefore cannot completely exclude that other binding areas outside of the selected one might also qualify as potential binding sites. The ligands were prepared using the implemented LigPrep module and the OLPS3 force field in possible states at pH 7.4 ± 1.0. The conformations of the docked ligands within an energy window of 2.5 kcal/mol were considered. For Glide docking, the following standard parameters were selected: receptor van der Waals scaling, 0.50; ligand van der Waals scaling, 0.50; a maximum of 20 poses per ligand. Residues within 5.0 Å of the ligand poses were refined, and the side chains were optimized. As precision setting XP (extra precision) was chosen. From the docking results, the binding poses of the agonists were sorted based on their IFD score and Prime Energy values. The poses are visually interpreted based on their electrostatic, hydrogen and hydrophobic interactions. Then the best docking pose was selected on the basis of their interactions matching the SARs of the agonists..

**6. Molecular dynamics simulations.** The receptor-ligand complexes for molecular dynamics simulations were prepared using the membrane builder module of CHARMM–GUI.[47] The complexes were embedded in a 2-oleoyl-1-palmitoyl-sn-glycero-3-phosphocholine (POPC) lipid bilayer according to the suggested orientation reported in the Orientations of Proteins in Membranes (OPM) database for the template structure (PDB ID: 4PXZ).[48] Then the prepared complexes were solvated with transferable intermolecular potential 3P (TIP3P) water molecules and neutralized by adding $Na^+/Cl^-$ counter ions to a final concentration of 0.154 M. All simulations were performed using the CHARMM C36p force field.[49] During the simulations, non-bonded interactions were gradually switched off at 10 Å and the long-range electrostatic interactions were calculated using the particle-mesh Ewald method. The prepared complexes were equilibrated with the standard six-step process over 5 ns implemented in CHARMM-GUI during which constraints on lipid molecules were gradually released. Finally, an unrestrained production run was performed for 100 ns with 4 fs time step using ACEMD.[50] The stability of the complexes along the simulation of 100 ns was evaluated according to root mean square deviation (RMSD) by aligning the receptor complexes on the basis of the first trajectory frame as the reference.

## ASSOCIATED CONTENT

**Supporting Information.**

Spectral data of the newly synthesized compounds (**9**–**15**, **17**, **21**–**23**, **26**, **27**, **29**, **30**, **40**, **42**, **44**, **51**, **55**, **57**–**59**, **62** and **64**); $^{1}$H-NMR spectrum of compound **39**; $^{1}$H and $^{13}$C-NMR spectra of compounds **33**–**36**, **41**, **43** and **45**; LC-MS spectra of compounds (**1**, **33**–**36**, **39**, **41**, **43** and **45**); overall sequence alignment of the human GPR17 and the human $P2Y_{12}$ receptor; Ramachandran diagram of the human GPR17 model; sequence-structure compatibility of the human GPR17 model; comparison of amino acid sequences of mouse, rat and human GPR17; two-dimensional interaction diagram of **1** and **43**; comparison of the binding sites; molecular dynamics simulations of the receptor complexes; concentration–response curves of active compounds. Molecular formula strings are provided. Molecular dynamic simulation videos for compounds **1** and **43**.

## AUTHOR INFORMATION

### Corresponding Author

*For C.E.M.: phone, +49-228-73-2301; fax, +49-228-73-2567; E-mail, christa.mueller@uni-bonn.de.**ORCID**

Younis Baqi: 0000-0002-9659-8419

Thanigaimalai Pillaiyar: 0000-0001-5575-8896

Aliaa Abdelrahman: 0000-0001-5734-2165

Evi Kostenis: 0000-0001-8284-5514

Meryem Köse: 0000-0002-3391-3418

Vigneshwaran Namasivayam: 0000-0003-3031-3377

Christa E. Müller: 0000-0002-0013-6624

### Author contributions

[§]Y.B. and T.P. contributed equally

**Notes**

The authors declare no competing financial interest.

**ACKNOWLEDGMENTS**

Y.B. is grateful for Sultan Qaboos University (SQU) grant (SR/SCI/CHEM/15/01) and Arab-German Young Academy (AGYA) grants (AGYA_2017_TP_02, AGYA_2017_TP_07, & AGYA_2017_TP_13). T.P. thanks the Alexander von Humboldt foundation and Bayer Pharma for a postdoctoral fellowship. A.A., E.K. and C.E.M. were supported by the BMBF (German Federal Ministry for Education and Research) within the BioPharma initiative "Neuroallianz" and by UCB (Union Chimique Belge). K.R. was supported by Evangelisches Studienwerk e.V. (PhD scholarship). We would like to thank Stefanie Weyer and Katharina Sylvester for expert technical assistance and Schrödinger Inc. for providing the evaluation license.

**ABBREVIATIONS USED**

| | |
|---|---|
| ADP | Adenosine-5'-diphosphate |
| ATP | Adenosine-5'-triphosphate |
| cAMP | Cyclic Adenosine-5'-monophosphate |
| CHO | Chinese hamster ovary |
| CNS | Central nervous system |
| DMSO | Dimethyl sulfoxide |
| DOPE | Discrete Optimized Protein Energy |
| ECL | Extracellular loop |
| ESI-MS | Electrospray ionization mass spectrometry |
| FRET | Förster resonance energy transfer |
| FTIR | Fourier Transformation Infrared Spectroscopy |
| GPCR | G protein-coupled receptor |
| HBSS | Hank's balanced salt solution |

| | |
|---|---|
| HEK | Human embryonic kidney |
| HEPES | 4-(2-Hydroxyethyl)-1-piperazineethanesulfonic acid |
| HPLC | High-performance liquid chromatography |
| IFD | Induced Fit Docking |
| LC-MS | Liquid chromatography mass spectroscopy |
| m.p. | melting point |
| MDL-29,951 | 3-(2-Carboxyethyl)-4,6-dichloro-1*H*-indole-2-carboxylic acid |
| MeS | Methylthio |
| MOE | Molecular Operating Environment |
| NMR | Nuclear magnetic resonance |
| OPLS | Optimized Potentials for Liquid Simulations |
| OPM | Orientations of Proteins in Membranes |
| PDB | Protein Data Bank |
| POPC | 2-Oleoyl-1-palmitoyl-*sn*-glycero-3-phosphocholine |
| rt | room temperature |
| RMSD | root mean square deviation |
| RT-PCR | Real Time Polymerase Chain Reaction |
| SARs | Structure-activity relationships |
| THF | Tetrahydrofuran |
| TLC | Thin-layer chromatography |
| TM | Transmembrane region |

## ANCILLARY INFORMATION

Authors will release the atomic coordinates upon article publication.

## REFERENCES


1. Davenport, A.P.; Alexander, S.P.; Sharman, J.L.; Pawson, A.J.; Benson, H.E.; Monaghan, A.E.; Liew, W.C.; Mpamhanga, CP.; Bonner, T.I.; Neubig R.R.; Pin, J.P.; Spedding, M.; Harmar, A.J. International Union of Basic and Clinical Pharmacology. LXXXVIII. G protein-coupled receptor list: recommendations for new pairings with cognate ligands. *Pharmacol. Rev*. **2013**, *65*, 967–986.
2. Hauser, A.S.; Attwood, M.M.; Rask-Anders, M.; Schiöth, H. B.; Gloriam, D.E. Trends in GPCR drug discovery: new agents, targets and indications. *Nat. Rev. Drug Discov.* **2017**, *16*, 829–842.
3. Müller, C.E.; Schiedel, A.C.; Baqi, Y. Allosteric modulators of rhodopsin-like G protein-coupled receptors: opportunities in drug development. *Pharmacol. Ther*. **2012**, *135*, 292–315.
4. Hennen, S.; Peters, L.; Wang, H.; Spinrath, A.; Merten, N.; Blättermann, S.; Akkari, R.; Schrage, R.; Simon, K.; Schröder, R.; Schulz, D.; Vermeiren, C.; Zimmermann, K.; Kehraus, S.; Drewke, C.; Pfeifer, A.; König, G.M.; Mohr, K.; Gillard, M.; Müller, C.E.; Lu, Q.R.; Gomeza, J.; Kostenis, E. Decoding signaling and function of the orphan G protein-coupled receptor GPR17 with a small-molecule agonist. *Sci. Signal*. **2013**, *6*, ra93.
5. Ciana, P.; Fumagalli, M.; Trincavelli, M.L.; Verderio, C.; Rosa, P.; Lecca, D.; Ferrario, S.; Parravicini, C.; Capra, V.; Gelosa, P.; Guerrini, U.; Belcredito, S.; Cimino, M.; Sironi, L.; Tremoli, E.; Rovati, G.E.; Martini, C.; Abbracchio, M.P. The orphan receptor GPR17 identified as a new dual uracil nucleotides/cysteinyl-leukotrienes receptor. *EMBO J*. **2006**, *25*, 4615–4627.
6. Bläsius, R.; Weber, R.G.; Lichter, P.; Ogilvie; A. A novel orphan G protein-coupled receptor primarily expressed in the brain is localized on human chromosomal band 2q21. *J. Neurochem*. **1998**, *70*, 1357–1365.

7. Marucci, G.; Dal Ben, D.; Lambertucci, C.; Santinelli, C.; Spinaci, A.; Thomas, A.; Volpini, R.; Buccioni, M. The G protein-coupled receptor GPR17: Overview and update. *ChemMedChem* **2016**, *11*, 2567–2574.

8. Ou, Z.; Sun, Y.; Lin, L.; You, N.; Liu, X.; Li, H.; Ma, Y.; Cao, L.; Han, Y.; Liu, M.; Deng, Y.; Yao, L.; Lu, Q.R.; Chen, Y. Olig2-targeted G-protein-coupled receptor GPR17 regulates oligodendrocyte survival in response to lysolecithin-induced demyelination. *J. Neurosci*. **2016**, *36*, 10560–10573.

9. Fumagalli, M.; Lecca, D.; Abbracchio, M.P. CNS remyelination as a novel reparative approach to neurodegenerative diseases: The roles of purinergic signaling and the P2Y-like receptor GPR17. *Neuropharmacology* **2016**, *104*, 82–93.

10. Chen, Y.; Wu, H.; Wang, S.; Koito, H.; Li, J.; Ye, F.; Hoang, J.; Escobar, S.S.; Gow, A.; Arnett, H.A.; Trapp, B.D.; Karandikar, N.J.; Hsieh, J.; Lu, Q.R. The oligodendrocyte-specific G protein-coupled receptor GPR17 is a cell-intrinsic timer of myelination. *Nat. Neurosci*. **2009**, *12*, 1398–1406.

11. Simon, K.; Hennen, S.; Merten, N.; Blättermann, S.; Gillard, M.; Kostenis, E.; Gomeza, J. The orphan G protein-coupled receptor GPR17 negatively regulates oligodendrocyte differentiation via Gαi/o and its downstream effector molecules. *J. Biol. Chem*. **2016**, *291*, 705–718.

12. Fumagalli, M.; Lecca, D.; Coppolino, G.T.; Parravicini, C.; Abbracchio. M.P. Pharmacological properties and biological functions of the GPR17 receptor, a potential target for neuro-regenerative medicine. *Adv. Exp. Med. Biol.* – Protein Reviews, **2017**, *1051*, 169–192.

13. Maekawa, A.; Xing, W.; Austen, K.F.; Kanaoka, Y. GPR17 regulates immune pulmonary inflammation induced by house dust mites. *J. Immunol*. **2010**, *185*, 1846–1854.

14. Benned-Jensen, T.; Rosenkilde, M.M. Distinct expression and ligand-binding profiles of two contitutively active GPR17 splice variants. *Br. J. Pharmacol*. **2010**, *159*, 1092–1105.

15. Maekawaa, A.; Balestrieria, B.; Austena, K.F.; Kanaokaa, Y. GPR17 is a negative regulator of the cysteinyl leukotriene 1 receptor response to leukotriene D4. *Proc. Natl. Acad. Sci.* **2009**, *106*, 11685–11690.

16. Qi, A.D.; Harden, T.K.; Nicholas, R.A. Is GPR17 a P2Y/leukotriene receptor? examination of uracil nucleotides, nucleotide sugars, and cysteinyl leukotrienes as agonists of GPR17. *J. Pharmacol. Exp. Ther.* **2013**, *347*, 38–46.

17. Simon, K.; Merten, N.; Schröder, R.; Hennen, S.; Preis, P.; Schmitt, N.K.; Peters, L.; Schrage, R.; Vermeiren, C.; Gillard, M.; Mohr, K.; Gomeza, J.; Kostenis, E. The orphan receptor gpr17 is unresponsive to uracil nucleotides and cysteinyl leukotrienes. *Mol. Pharmacol*. **2017,** *91*, 518–532.

18. Baqi, Y.; Alshaibani, S.; Ritter, K.; Abdelrahman, A.; Spinrath, A.; Kostenis, E.; Müller, C.E. Improved synthesis of 4-/6-substituted 2-carboxy-1*H*-indole-3-propionic acid derivatives and structure–activity relationships as GPR17 agonists. *MedChemComm*, **2014**, *5*, 86–92.

19. Köse, M.; Ritter, K.; Thiemke, K.; Gillard, M.; Kostenis, E.; Müller, C.E. Development of [$^3$H]2-carboxy-4,6-dichloro-1*H*-indole-3-propionic acid ([$^3$H]PSB-12150): A useful tool for studying GPR17. *ACS Med. Chem. Lett*. **2014**, *5*, 326–330.

20. Salituro, F.G.; Harrison, B.L.; Baron, B.M.; Nyce, P.L.; Stewart, K.T.; Kehne, J.H.; White, H.S.; McDonald, I.A. 3-(2-Carboxyindol-3-yl)propionic acid-based antagonists of the NMDA (N-methyl-D-aspartic acid) receptor associated glycine binding site. *J. Med. Chem*. **1992**, *35*, 1791–1799.

21. Salituro, F.G.; Harrison, B.L.; Baron, B.M.; Nyce, P.L.; Stewart, K.T.; McDonald, I.A. 3-(2-Carboxyindol-3-yl)propionic acid derivatives: antagonists of the strychnine-insensitive glycine receptor associated with the N-methyl-D-aspartate receptor complex. *J. Med. Chem*. **1990**, *33*, 2944–2946.

22. Akladios, F.N.; Nadvi, N.A.; Park, J.; Hanrahan, J.R.; Kapoor, V.; Gorrell, M.D.; Church, W.B. Design and synthesis of novel inhibitors of human kynurenine aminotransferase-I. *Bioorg. Med. Chem. Lett.* **2012**, *22*, 1579–1581.

23. Menciu, C.; Duflos, M.; Fouchard, F.; Le Baut, G.; Emig, P.; Achterrath, U.; Szelenyi, I.; Nickel, B.; Schmidt, J.; Kutscher, B.; Günther, E. New N-(pyridin-4-yl)-(indol-3-yl)acetamides and propanamides as antiallergic agents. *J. Med. Chem*. **1999**, *42*, 638–648.

24. Takahashi, K.; Kasai, M.; Ohta, M.; Shoji, Y.; Kunishiro, K.; Kanda, M.; Kurahashi, K.; Shirahase, H. Novel indoline-based acyl-CoA:cholesterol acyltransferase inhibitor with antiperoxidative activity: improvement of physicochemical properties and biological activities by introduction of carboxylic acid. *J. Med. Chem*. **2008**, *51*, 4823–4833.

25. Tayyem, R.F.; Zalloum, H.M.; Elmaghrabi, M.R.; Yousef, A.M.; Mubarak, M.S. Ligand-based designing, in silico screening, and biological evaluation of new potent fructose-1,6-bisphosphatase (FBPase) inhibitors. *Eur. J. Med. Chem.* **2012**, *56*, 70–95.

26. Baqi, Y.; Müller, C.E. Synthesis of alkyl- and aryl amino-substituted anthraquinone derivatives by microwave-assisted copper(0)-catalyzed Ullmann coupling reactions. *Nat. Protoc*. **2010**, *5*, 945–953.

27. Fujioka, M.; Omori, N. Subtleties in GPCR drug discovery: a medicianl chemistry perspective. *Drug Discov. Today* **2012**, *17*, 1133–1138.

28. Zhang, J.; Zhang, K.; Gao, Z.G.; Paoletta, S.; Zhang, D.; Han, G.W.; Li, T.; Ma, L.; Zhang, W.; Müller, C.E.; Yang, H.; Jiang, H.; Cherezov, V.; Katritch, V.; Jacobson, K.A.; Stevens, R.C.; Wu, B.; Zhao, Q. Agonist-bound structure of the human $P2Y_{12}$ receptor. *Nature* **2014**, *509*, 119–122.

29. Zhang, K.; Zhang, J.; Gao, Z.G.; Zhang, D.; Zhu, L.; Han, G.W.; Moss, S.M.; Paoletta, S.; Kiselev, E.; Lu, W.; Fenalti, G.; Zhang, W.; Müller, C.E.; Yang, H.; Jiang, H.; Cherezov, V.; Katritch, V.; Jacobson, K.A.; Stevens, R.C.; Wu, B.; Zhao, Q. Structure of the human $P2Y_{12}$ receptor in complex with an antithrombotic drug. *Nature* **2014**, *509*, 115–118.

30. Parravicini, C.; Ranghino, G.; Abbracchio, M.P.; Fantucci, P. GPR17: molecular modeling and dynamics studies of the 3-D structure and purinergic ligand binding features in comparison with P2Y receptors. *BMC Bioinformatics* **2008**, *9*, 263.

31. Eberini, I.; Daniele, S.; Parravicini, C.; Sensi, C.; Trincavelli, M.L.; Martini, C.; Abbracchio, M.P. In silico identification of new ligands for GPR17: a promising therapeutic target for neurodegenerative diseases. *J. Comput. Aided Mol. Des.* **2011,** *25*, 743–752.

32. Sali, A.; Blundell, T. L. Comparative protein modelling by satisfaction of spatial restraints. *J. Mol. Biol.* **1993**, *234*, 779–815.

33. Webb, B.; Sali, A. Protein structure modeling with MODELLER. *Methods Mol. Biol.* **2014**, *1137*, 1–15.

34. Molecular Operating Environment (MOE 2014.09); Chemical Computing Group: Montreal, Quebec, Canada, **2014**.

35. Hillmann, P.; Ko, G. Y.; Spinrath, A.; Raulf, A.; von Kügelgen, I.; Wolff, S. C.; Nicholas, R. A.; Kostenis, E.; Höltje, H. D.; Müller, C. E. Key determinants of nucleotide-activated G protein-coupled P2Y2 receptor function revealed by chemical and pharmacological experiments, mutagenesis and homology modeling. *J. Med. Chem.* **2009**, *52*, 2762–2775.

36. Rafehi, M.; Malik, E.M.; Neumann, A.; Abdelrahman, A.; Hanck, T.; Namasivayam, V.; Müller, C.E.; Baqi, Y. Development of potent and selective antagonists for the UTP-activated $P2Y_4$ receptor. *J. Med. Chem.* **2017**, *60*, 3020–3038.

37. Rafehi, M.; Burbiel, J.C.; Attah, I.Y.; Abdelrahman, A. Müller, C.E. Synthesis, characterization, and in vitro evaluation of the selective P2Y2 receptor antagonist AR-C118925. *Purinergic Signal*. **2017**, *13*, 89–103.

38. Berman, H.M.; Westbrook, J.; Feng, Z.; Gilliland, G.; Bhat, T.N.; Weissig, H.; Shindyalov, I. N.; Bourne, P.E. The protein data bank. *Nucleic Acids Res.* **2000**, *28*, 235–242.

39. The Uniprot Consortium. UniProt, a hub for protein information. *Nucleic Acids Res.* **2015**, *43* (Database issue), D204–D212.

40. Sievers, F.; Wilm, A.; Dineen, D.; Gibson, T.J.; Karplus, K.; Li, W.; Lopez, R.; McWilliam, H.; Remmert, M.; Söding, J.; Thompson, J.D.; Higgins, D.G. Fast, scalable generation of high-quality protein multiple sequence alignments using Clustal Omega. *Mol. Syst. Biol*. **2011**, *7*, 539.

41. Lovell, S.C.; Davis, I.W.; Arendall, W.B.3rd; de Bakker, P.I.; Word, J.M.; Prisant, M.G.; Richardson, J.S.; Richardson, D.C. Structure validation by Calpha geometry: phi, psi and Cbeta deviation. *Proteins* **2003,** *50*, 437–450.

42. Ramachandran, G.N.; Ramakrishnan, C.; Sasisekharan, V.; Stereochemistry of polypeptide chain configurations. *J. Mol. Biol.* **1963**, *7*, 95–99.

43. Wiederstein, M.; Sippl, M.J. ProSA-web: interactive web service for the recognition of errors in three-dimensional structures of proteins. *Nucleic Acids Res.* **2007**, *35*, W407–W410.

44. Friesner, R.A.; Banks, J.L.; Murphy, R.B.; Halgren, T.A.; Klicic, J.J.; Mainz, D.T.; Repasky, M.P.; Knoll, E.H.; Shaw, D.E.; Shelley, M.; Perry, J.K.; Francis, P.; Shenkin, P.S. Glide, a new approach for rapid, accurate docking and scoring. 1. Method and assessment of docking accuracy. *J. Med. Chem.* **2004**, *47*, 1739–1749.

45. Halgren, T.A.; Murphy, R.B.; Friesner, R.A.; Beard, H.S.; Frye, L.L.; Pollard, W.T.; Banks, J.L. Glide, a new approach for rapid, accurate docking and scoring. 2. Enrichment factors in database screening. *J. Med. Chem.* **2004**, *47*, 1750–1759.

46. Sherman, W.; Day, T.; Jacobson, M.P.; Friesner, R.A.; Farid, R. Novel procedure for modeling ligand/receptor induced fit effects. *J. Med. Chem.* **2006**, *49*, 534–553.

47. Jo, S.; Lim, J. B.; Klauda, J. B.; Im, W., CHARMM-GUI Membrane Builder for mixed bilayers and its application to yeast membranes. *Biophys. J.* **2009,** *97*, 50–58.

48. Klauda, J. B.; Monje, V.; Kim, T.; Im, W., Improving the CHARMM force field for polyunsaturated fatty acid chains. *J. Phys. Chem. B* **2012,** *116*, 9424–9231.

49. Lomize, M. A.; Lomize, A. L.; Pogozheva, I. D.; Mosberg, H. I., OPM: orientations of proteins in membranes database. *Bioinformatics* **2006,** *22*, 623–635.

50. Harvey, M. J.; Giupponi, G.; Fabritiis, G. D., ACEMD: Accelerating biomolecular dynamics in the microsecond time scale. *J. Chem. Theory Comput.* **2009,** *5*, 1632–1639.

## Table of Contents Graphic

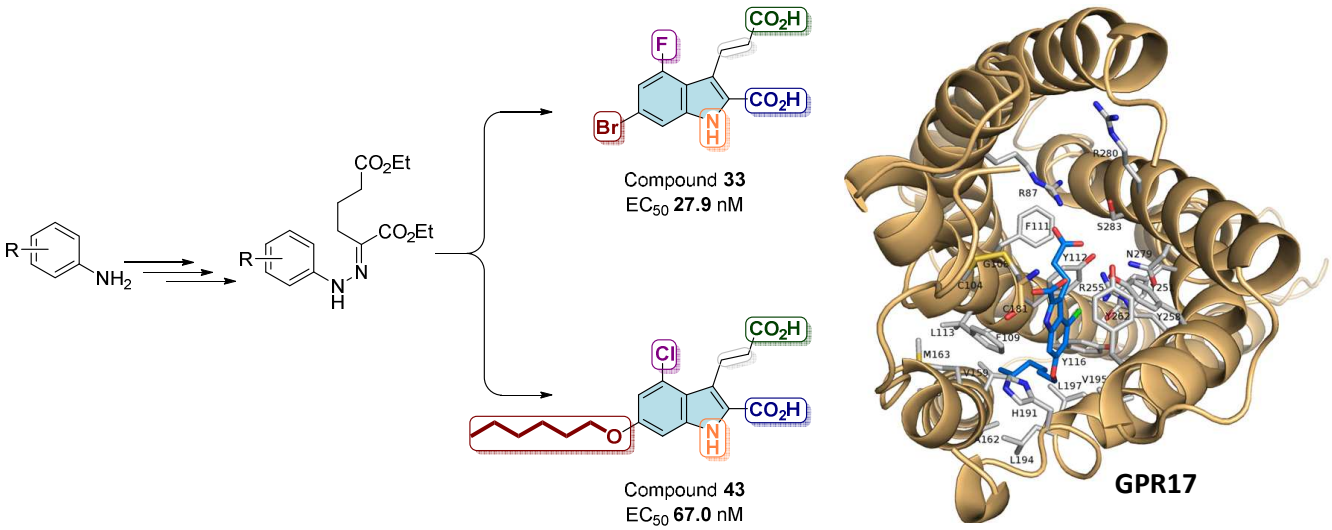

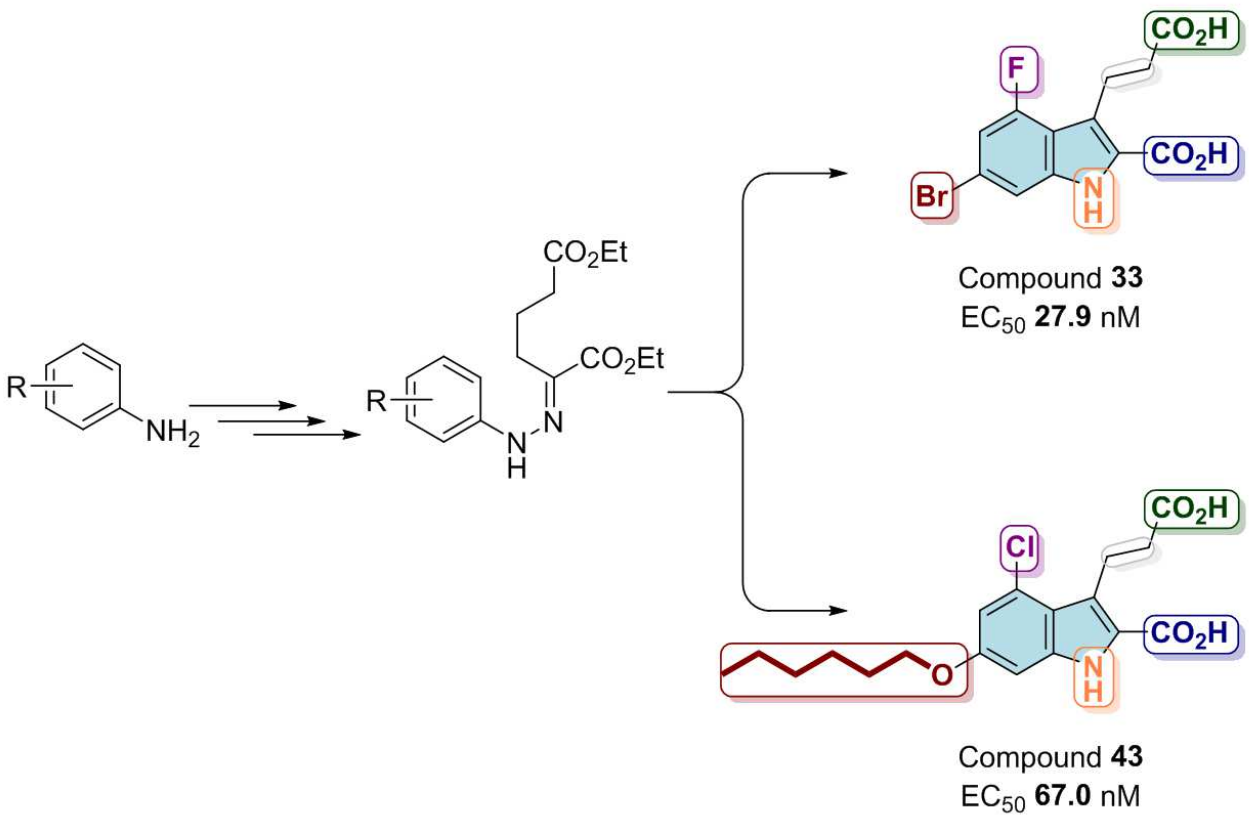
R
NH2
CO2Et
CO2Et
R
N
N
H
F
CO2H
Br
CO2H
N
H
Compound 33
EC50 27.9 nM
Cl
CO2H
O
CO2H
N
H
Compound 43
EC50 67.0 nM

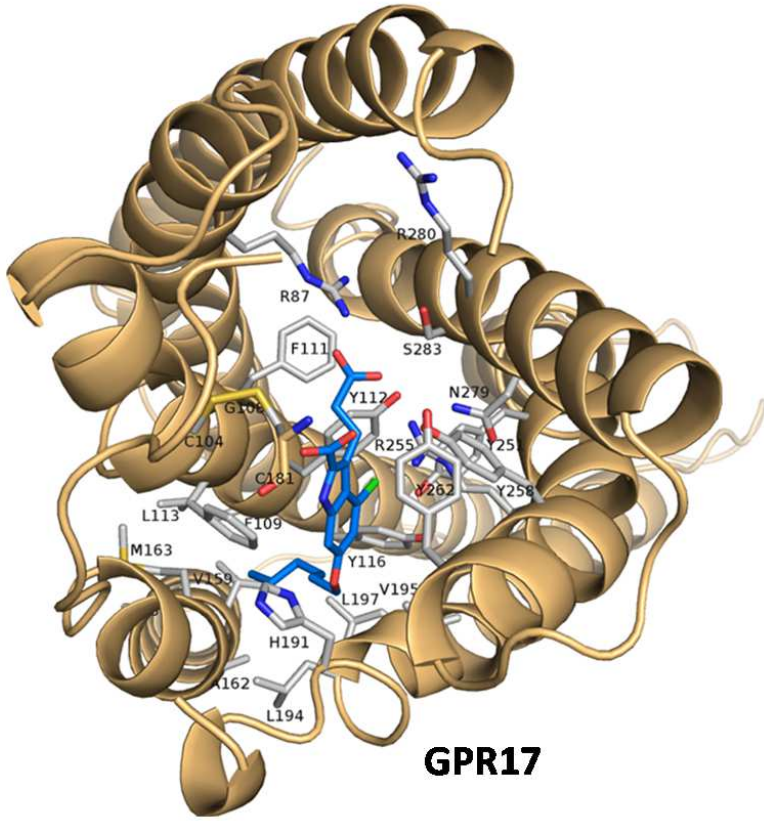
R280
R87
F111
S283
N279
Y112
G108
C104
R255
C181
Y262
Y258
L113
F109
M163
Y116
V159
L197
V195
H191
K162
L194
GPR17